Aerosol Science and Technology, 46:258–271, 2012

ISSN: 0278-6826 print / 1521-7388 online
DOI: 10.1080/02786826.2011.620041

Evaluation of Composition-Dependent Collection Efficiencies for the Aerodyne Aerosol Mass Spectrometer using Field Data

Ann M. Middlebrook,[1] Roya Bahreini,[1,2] Jose L. Jimenez,[2,3] and Manjula R. Canagaratna[4]

[1]*NOAA Earth System Research Laboratory, Chemical Sciences Division, Boulder, Colorado, USA*
[2]*University of Colorado, Cooperative Institute for Research in Environmental Studies (CIRES), Boulder, Colorado, USA*
[3]*Department of Chemistry and Biochemistry, University of Colorado, Boulder, Colorado, USA*
[4]*Aerodyne Research Inc., Billerica, Massachusetts, USA*

In recent years, Aerodyne aerosol mass spectrometers (AMS) have been used in many locations around the world to study the size-resolved, nonrefractory chemical composition of ambient particles. In order to obtain quantitative data, the mass or (number) of particles detected by the AMS relative to the mass (or number) of particles sampled by the AMS, i.e., the AMS collection efficiency (*CE*) must be known. Previous studies have proposed and used parameterizations of the AMS *CE* based on the aerosol composition and sampling line relative humidity. Here, we evaluate these parameterizations by comparing AMS mass concentrations with independent measurements of fine particle volume or particle-into-liquid sampler (PILS) ion chromatography measurements for 3 field campaigns with different dominant aerosol mixtures: (1) acidic sulfate particles, (2) aerosol containing a high mass fraction of ammonium nitrate, and (3) aerosol composed of primarily biomass burning emissions. The use of the default *CE* of 0.5 for all campaigns resulted in 81–90% of the AMS speciated and total mass concentrations comparing well with fine particle volume or PILS measurements within experimental uncertainties, with positive biases compared with a random error curve. By using composition-dependent *CE* values (sometimes as a function of size) which increased the *CE* for the above aerosol types, the fraction of data points within the measurement uncertainties increased to more than 92% and the mass concentrations decreased by ∼5–15% on an average. The *CE* did not appear to be significantly dependent on changes in organic mass fraction although it was substantial in the 3 campaigns (47, 30, and 55%).

Received 23 March 2011; accepted 1 August 2011.

We thank Chuck Brock, Adam Wollny, Carlos Gallar, Julie Cozic, Shuka Schwarz, Ryan Spackman, Ru-Shan Gao, Laurel Watts, David Fahey, Brendan Matthew, Kristen Schulz, Derek Coffman, Trish Quinn, Tim Onasch, Frank Drewnick, and the AMS user community for providing data and/or useful discussions. JLJ was supported by NASA NNX08AD39G and NOAA NA08OAR4310565.

Address correspondence to Ann M. Middlebrook, NOAA Earth System Research Laboratory, Chemical Sciences Division, 325 Broadway, R/CSD2, Boulder, CO 80305, USA. E-mail: Ann.M.Middlebrook@noaa.gov

[Supplementary materials are available for this article. Go to the publisher's online edition of *Aerosol Science and Technology* to view the free supplementary files.]

INTRODUCTION

Current uncertainties of aerosol impacts on climate and human health have driven the development of advanced instrumentation that allows rapid and sensitive measurements of aerosol chemical species. The Aerodyne Aerosol Mass Spectrometers (AMS) or AMS instruments (Aerodyne Research Inc., Billerica, MA) (Jayne et al. 2000; Canagaratna et al. 2007) are currently the most commonly used research instrument in this category, and they are often used in the field and laboratory studies across the world (Zhang et al. 2007a; Jimenez et al. 2009). The general operation of AMS instruments has been described elsewhere (Jayne et al. 2000; Allan et al. 2003b; Jimenez et al. 2003; Drewnick et al. 2005; DeCarlo et al. 2006; Canagaratna et al. 2007). Briefly, particles are transmitted into the AMS detection region using an aerodynamic focusing lens, where they impact an inverted-cone porous-tungsten vaporizer typically held at 600°C, and volatilize, with the vapors being analyzed by electron ionization mass spectrometry. The net overall particle transmission and detection efficiency is called the collection efficiency (*CE*) and is expressed by the product of 3 terms (Huffman et al. 2005):

$$CE(d_{va}) = E_L(d_{va}) \times E_S(d_{va}) \times E_b(d_{va}) \qquad [1]$$

where E_L is the transmission efficiency of the aerodynamic lens for spherical particles, E_S captures the loss of transmission

due to particle nonsphericity which causes the particle beam to broaden, and E_b is the efficiency with which a particle that impacts the vaporizer is detected. E_L is largely dependent on particle size (vacuum aerodynamic diameter or d_{va}) (DeCarlo et al. 2004) and the lens design and operating pressure (Jayne et al. 2000; Zhang et al. 2004; Liu et al. 2007; Bahreini et al. 2008). For ambient particles transmitted through the AMS lens, laboratory, and field measurements have shown that even though ambient particles are often slightly nonspherical in the AMS, the losses due to particle nonsphericity are minor (Huffman et al. 2005; Quinn et al. 2006; Salcedo et al. 2007).

E_b is dependent on the degree to which particles bounce when they impact the vaporizer. Field experiments suggested (Allan et al. 2004a; Quinn et al. 2006) and laboratory experiments demonstrated (Matthew et al. 2008) that the last term of the AMS *CE*, E_b, is a function of particle phase. In general, previous studies indicate that particles with liquid surfaces have higher AMS *CE* than those that are solid. There are 4 main factors which influence particle phase in the AMS: relative humidity in the sampling line, acidity/neutralization of the sulfate content, ammonium nitrate content, and organic liquid content. Thus far, only the inorganic species have been studied extensively in the laboratory. Since particles typically lose all or much of the particle-phase water in the AMS inlet and vacuum system (Zelenyuk et al. 2006; Matthew et al. 2008), the sampling line *RH* must be above 90% *RH* for the particles to remain liquid when impacting on the vaporizer (Matthew et al. 2008). At lower *RH*, sulfuric acid particles are liquid whereas the phase of ammonium bisulfate and sulfate particles in the atmosphere depends on whether or not the particles were initially dry or hydrated (Tang 1980). Indeed, field measurements of particulate phase suggest that ambient sulfate aerosols are more frequently metastable liquids between 45 and 75% *RH* (Rood et al. 1989) or that particles can retain water at *RH* lower than the deliquescence point (Khlystov et al. 2005; Engelhart et al. 2011), although particles in that *RH* range may lose most or all of their water in the AMS. Ammonium nitrate is a metastable liquid in the atmosphere at any sampling line *RH*. For pure ammonium sulfate and sulfate-dominated ambient particles, E_b increases with sampling line *RH* above the deliquescence *RH* (Allan et al. 2004a; Matthew et al. 2008) as well as with the deposition of thick coatings of organic liquids (Matthew et al. 2008). The *CE* for dry sulfate particles also increases with aerosol acidity (Quinn et al. 2006) and increasing nitrate content (Weimer et al. 2006; Crosier et al. 2007; Matthew et al. 2008; Nemitz et al. 2011). In all cases, the trends are qualitatively explained by changes in particle phase.

Organic particles can be either liquid or solid, but theory predicts that mixtures of inorganic salts and dicarboxylic acids will remain in a liquid phase under ambient conditions (Marcolli et al. 2004). Recent results suggest that aged ambient organic aerosols have very low volatility, which calls into question whether they form a liquid phase in the atmosphere (Huffman et al. 2009; Cappa and Jimenez 2010). Liquid organic particles are collected with $E_b = 1$ (Matthew et al. 2008), however, ambient organic-dominated particles have typical $E_b \sim 0.5$ (Salcedo et al. 2006; DeCarlo et al. 2008; Kleinman et al. 2008; Aiken et al. 2009) which suggests that they are not liquid in the AMS.

For some field studies, apparent *CE* values have been determined with the ambient data by comparing AMS mass loadings for the individual species with other particulate chemical measurements such as particle-into-liquid samplers (PILS) with ion chromatography analysis (Weber et al. 2001; Takegawa et al. 2005) and online OC analyzers (Takegawa et al. 2005), or by comparing the total AMS mass loadings with total apparent volume- or total mass-based instruments such as scanning mobility particle sizers (Quinn et al. 2006) or tapered element oscillating microbalances (TEOM) (Allan et al. 2004a; Drewnick et al. 2004; Hogrefe et al. 2004; Weimer et al. 2006). Many field studies reported that reasonable agreement and linear correlations were obtained with other measurements by using a *CE* of 0.5 (Allan et al. 2003a; Alfarra et al. 2004; Topping et al. 2004; Takegawa et al. 2005; Salcedo et al. 2006; Aiken et al. 2009; Timonen et al. 2010). In several field studies, the *CE* value was estimated from sulfate comparisons (Drewnick et al. 2004; de Gouw et al. 2005; Takegawa et al. 2005; Venkatachari et al. 2006; Weimer et al. 2006; Kondo et al. 2007; de Gouw et al. 2008). In such cases, the AMS organic mass calculated using the *CE* value estimated from only the sulfate mass intercomparisons was still linearly-correlated with independent organic carbon measurements with reasonable average organic mass to organic carbon ratios of 1.7 ± 0.3 (de Gouw et al. 2005; Takegawa et al. 2005; Venkatachari et al. 2006; Kondo et al. 2007; de Gouw et al. 2008). These results suggest that the observed *CE* of $\sim$0.5 for most environments and chemical compositions is valid because ambient particles are solid in the AMS (Matthew et al. 2008) and are internally mixed (Murphy et al. 2006; Zhang et al. 2007a).

AMS instruments with *in situ* light-scattering detection have the potential to provide a direct measurement of *CE* (Cross et al. 2009; Slowik et al. 2010). However, particles must be large enough to scatter light in the instrument ($\sim$215 nm in diameter), provide enough signal from the single particle mass spectra to count individual particles, and evaporate in 3 ms or less, which make the results not directly applicable to the most commonly used MS-mode in which smaller particles and slower-evaporating species are still detected. More studies involving this method are needed to evaluate its use with ambient aerosols.

While a single *CE* value can be used to obtain speciated aerosol mass concentrations in many ambient environments, some field measurement comparisons suggest that individual pollution events are best captured by introducing composition-dependent *CE* values. Previous studies have developed empirical formulations of inorganic composition-dependent *CE* based on field comparisons (Quinn et al. 2006; Crosier et al. 2007). Here, we use data from 3 different field studies to compare AMS mass, using the default $CE = 0.5$, with external

measurements, to support parameterizations of *CE* as a function of composition, and finally to show case studies of how these parameterizations improved the overall comparisons with data from other instruments. Since E_L is explicitly taken into account for these comparisons, E_S is assumed to be 1 based on previous beam width measurements of ambient particles (Huffman et al. 2005; Salcedo et al. 2007), and E_b for a single component has not shown size-dependence in the laboratory (Matthew et al. 2008), the apparent *CE* should be equal to E_b.

FIELD DATA AND INSTRUMENTATION

Three sets of field data are used in this work: an airborne study based in Houston, TX during September–October 2006 (Texas Air Quality Study/Gulf of Mexico Atmospheric Composition and Climate Study, TexAQS-II/GoMACCS), a ground-based study in Boulder, CO during January–February 2005, and an airborne study above northern Alaska during April 2008 (Aerosol, Radiation, and Cloud Processes affecting Arctic Climate, ARCPAC). The AMS instrument used in the ground-based study was equipped with a quadrupole mass spectrometer, whereas a compact-time-of-flight (C-ToF) mass spectrometer was used with a pressure-controlled inlet for the airborne studies (Bahreini et al. 2008). In all 3 datasets analyzed here, the instrument was alternated between the bulk mass spectral mode (MS) and the particle time-of-flight mode (PToF). As shown below and in the supplemental material (Figures S1–S3), these 3 sets of field data spanned a wide range of aerosol composition in terms of the mass fractions of different species.

The AMS inlet flow rate, particle velocity, nitrate ionization efficiency, and relative ionization efficiency for ammonium were calibrated before, during, and after the field studies with standard procedures (e.g., Canagaratna et al. 2007). MS and PToF data were recorded every 2.5 min for the ground-based study and every 10–15 s for the airborne studies. The data were processed using custom software written in Igor Pro (Wavemetrics Inc.) and developed for the AMS and shared across the AMS community (Allan et al. 2004b; DeCarlo et al. 2006). The mass loadings for each species (C_s in μg m^{-3}) were calculated in the following manner (adapted from (Jimenez et al. 2003) and Equation 7 in (Allan et al. 2004b)):

$$C_s = 10^{12} \frac{MW_{\mathrm{NO_3}}}{CE_s RIE_s IE_{\mathrm{NO_3}} Q N_A} \sum_i I_{s,i} \qquad [2]$$

where MW_{NO3} is the molecular weight of nitrate (62 g mol^{-1}), CE_s is the collection efficiency of species s, IE_{NO3} is the ionization, transmission, and ion detection efficiency of nitrate (in ions molec^{-1}, typically shortened as "ionization efficiency"), RIE_s is the ionization efficiency of species s relative to the ionization efficiency of nitrate, Q is the volumetric sample flow rate into the instrument (in cm^3 s^{-1}), N_A is Avogadro's number, I_s is the measured ion rate in the partial mass spectra for species s (in ions s^{-1}), where all of the *m/z* fragments (i) in the partial mass spectra are summed for species s. For some species, the calculation of partial mass spectra relies on fragmentation patterns determined in the laboratory and known isotopic ratios (Allan et al. 2004b). The factor of 10^{12} converts the units from g cm^{-3} to μg m^{-3}. The uncertainty in *CE* is around 30% (2σ) and it dominates the uncertainty for individual species (Bahreini et al. 2009). For organic material, the uncertainty in the organic *RIE* is around 20% (2σ) and is also a major contributor to its uncertainty (Bahreini et al. 2009). The propagated, overall uncertainty for the total AMS mass concentration is 20–35% (2σ) (Bahreini et al. 2009). See Supplementary Information section S1 of Bahreini et al. (2009) for details on uncertainty propagation. Here we used 30% uncertainty in the AMS total mass for the propagation of the combined measurement uncertainties between the AMS and UHSAS (ultra-high sensitivity aerosol spectrometer) or PILS.

The AMS detection limits were determined periodically during each field study by placing a filter in front of the AMS inlet, averaging the mass concentrations for each species using the default *CE*, and multiplying the resulting standard deviations by 3. Only data where all mass concentrations were greater than 3 times the detection limit were used in the results reported here. This effectively removes a bias toward larger errors for data where the mass concentrations were close to the detection limits.

For the fine particle volume measurements in the airborne studies, an ultra-high sensitivity aerosol spectrometer (UHSAS, Droplet Measurement Technologies, Boulder, CO) was used to measure the particle number distribution as a function of optical diameter, from which the apparent fine particle volume is calculated and reported (here for dry particles). The UHSAS was operated at ambient relative humidity in the sampling line on the aircraft, which was the same sampling line relative humidity as the AMS. The conditions in the AMS inlet cause additional drying that can change the phase of the particles from what they were in the sampling line (Matthew et al. 2008). The UHSAS instrument was calibrated with monodisperse, dry, ammonium sulfate particles, which have a known index of refraction. Each UHSAS bin of scattered light intensity was converted to particle size, based on the dry, ammonium sulfate index of refraction. The UHSAS volume was computed from the number distribution by assuming spherical particles. Mass was calculated from volume by using the AMS composition data to estimate the average density. The size range for the UHSAS is 0.06–1 microns. Uncertainty in size due to estimates of the actual refractive index (likely between 1.4 to 1.6 without an imaginary component) lead to ~10–15% uncertainty in diameter. This is the largest component of the 30–45% uncertainties in volume from the UHSAS (Brock et al. 2011).

To account for particle transmission losses in the AMS lens, the measured AMS lens transmission curve (Bahreini et al. 2008) was applied to the fine particle number distributions. The fine particle mass reported here therefore takes the lens transmission curve into account. Note that particle losses in the AMS lens can otherwise be incorrectly attributed to particle

bounce losses. Accurately accounting for the lens transmission efficiency is thus critical in comparisons of AMS mass concentrations with other measurements of the individual species. Here the additional mass measured by the UHSAS and not measured by the AMS due to lens transmission losses was at most 10% and typically less than 5%. Measurement uncertainties (2σ) for the UHSAS particle volume data were 30% for TexAQS (Bahreini et al. 2009) and +45/–31% for ARCPAC (Brock et al. 2011).

Ion chromatography was performed on aerosol samples collected with a PILS (Weber et al. 2001) and high-quality PILS measurements were available only for the Boulder study. For the data described here, the PILS system was operated with a 1 micron impactor on the sampling line which is similar to the upper limit of particles transmitted by the AMS lens. Particulate black carbon (BC) mass concentrations were obtained in the 2 airborne studies with a single-particle soot photometer (SP2) instrument (Schwarz et al. 2006). The size range measured by the SP2 instrument depends on particle density and is 0.07–0.50 μm mass-equivalent diameter assuming a BC density of 1.8 g cm^{-3} (Park et al. 2004). Experimental uncertainties (2σ) in the PILS and BC measurements are 10% (Weber et al. 2001) and 15% (Schwarz et al. 2006), respectively.

The AMS mass concentrations were compared with the other measurements in 2 ways: the AMS total plus BC mass was divided by the mass estimated from the UHSAS fine particle volume, or the AMS nitrate plus sulfate mass was divided by the nitrate plus sulfate mass from the PILS-IC system. The fine particle mass was obtained by multiplying the fine particle volume transmitted into the AMS by the density estimated from the AMS and BC composition. The mass-weighted density (ρ) was calculated using $\rho_{org} = 1.25$ g cm^{-3} (for TexAQS) or 1.3 g cm^{-3} (for ARCPAC), $\rho_{inorg} = 1.75$ g cm^{-3} (primarily dry ammonium sulfate, (Perry and Green 1997)), and $\rho_{BC} = 1.8$ g cm^{-3} (Park et al. 2004), for organic mass, inorganic mass, and BC, respectively. This calculation is not very sensitive to the density of BC because its mass fraction was nearly always less than 5%. The density for organic material is consistent with recent density measurements of ambient organic and biogenic secondary organic aerosol which have been determined in 3 independent studies as 1.27, 1.22–1.28, and 1.3 ± 0.1 g cm^{-3} (Cross et al. 2007; Zelenyuk et al. 2008; Kiendler-Scharr et al. 2009).

In this work, we develop and evaluate empirical parameterizations for *CE* to calculate bulk ensemble mass concentrations. Thus, some of the variability in the estimated *CE* could indeed be due to external versus internal mixing issues. The standard AMS instrument does not have a direct means of evaluating the mixing state of the particles, but differences in speciated size distributions can be indicative of different degrees of internal mixing. Here, the Boulder dataset and a few events in the TexAQS data showed distinctly different speciated size distributions. We have corrected for this effect on the bulk mass concentrations by using a size dependent *CE*. For the ARCPAC dataset and most of the TexAQS dataset where size dependent parameterizations were not needed, internal mixing is supported by other measurements (Asa-Awuku et al. 2011; Brock et al. 2011). Most of the submicron aerosol mass in these 3 field studies was either nonrefractory species or BC. For the Boulder study, about 99% of the ions measured with PILS were potentially measured by the AMS (chloride, nitrate, sulfate, and ammonium) and less than 2% were refractory species (sodium, calcium, magnesium, plus potassium). The number fraction of mineral dust and sea salt was always less than 10% of fine (<0.7 micron) aerosols in the ARCPAC study, with the exception of the Arctic boundary layer aerosols which had a slightly higher fraction of sea salt (Brock et al. 2011). Data with a clear influence of dust during ARCPAC was identified by comparisons of the AMS total mass to aerosol extinction data and removed from this analysis. Unfortunately, no comparable direct information about nonrefractory species was obtained during the TexAQS field study. The fact that the resulting correlation between AMS + BC mass and fine particle mass is good, with only a few outliers (see Figures S5–S6), suggests that dust or sea salt were not significant components of the fine particle mass.

RESULTS AND DISCUSSION

Evaluation of the Default AMS *CE*

Mass concentrations are typically calculated with a default $CE = 0.5$ for most ambient environments. Here, datasets from 3 field campaigns (TexAQS, Boulder, CO, and ARCPAC) are used to examine the appropriateness of the default *CE* and parameterizations of *CE* based on chemical composition. Figure 1 shows histograms of either (1) the ratio of the AMS total mass (using the default *CE*) plus BC mass to fine particle mass (M_{fine}), or (2) the AMS nitrate plus sulfate mass divided by the PILS nitrate plus sulfate mass for all 3 field studies. The propagated uncertainties (2σ) for the combined instrument mass ratios are 45% for TexAQS, 45% for Boulder, and +56/–46% for ARCPAC and 95.5% of the mass ratios are expected to cluster around 1.0 within these measurement uncertainties. The Gaussian random error curves for each study based on the combined measurement uncertainties are included with the histograms in Figure 1. More than 81% of the data fall within these combined measurement uncertainties (Table 1), which is consistent with the observation of a *CE* around 0.5 in most ambient measurement campaigns. However, significant fractions of all 3 datasets (12% for TexAQS, 19% for Boulder, and 18% for ARCPAC) are beyond the combined uncertainties, while the expected percentage due to random effects would be less than 5%. Most of the data points that were outside the combined measurement uncertainties were on the right-hand side of the random error curve (Figure 1), suggesting a systematic positive bias for a subset of the data. The ratios of speciated mass to fine particle mass that lie well above 1.0 correspond to pollution events or compositional differences for which composition-dependent parameterization of *CE* may be needed.

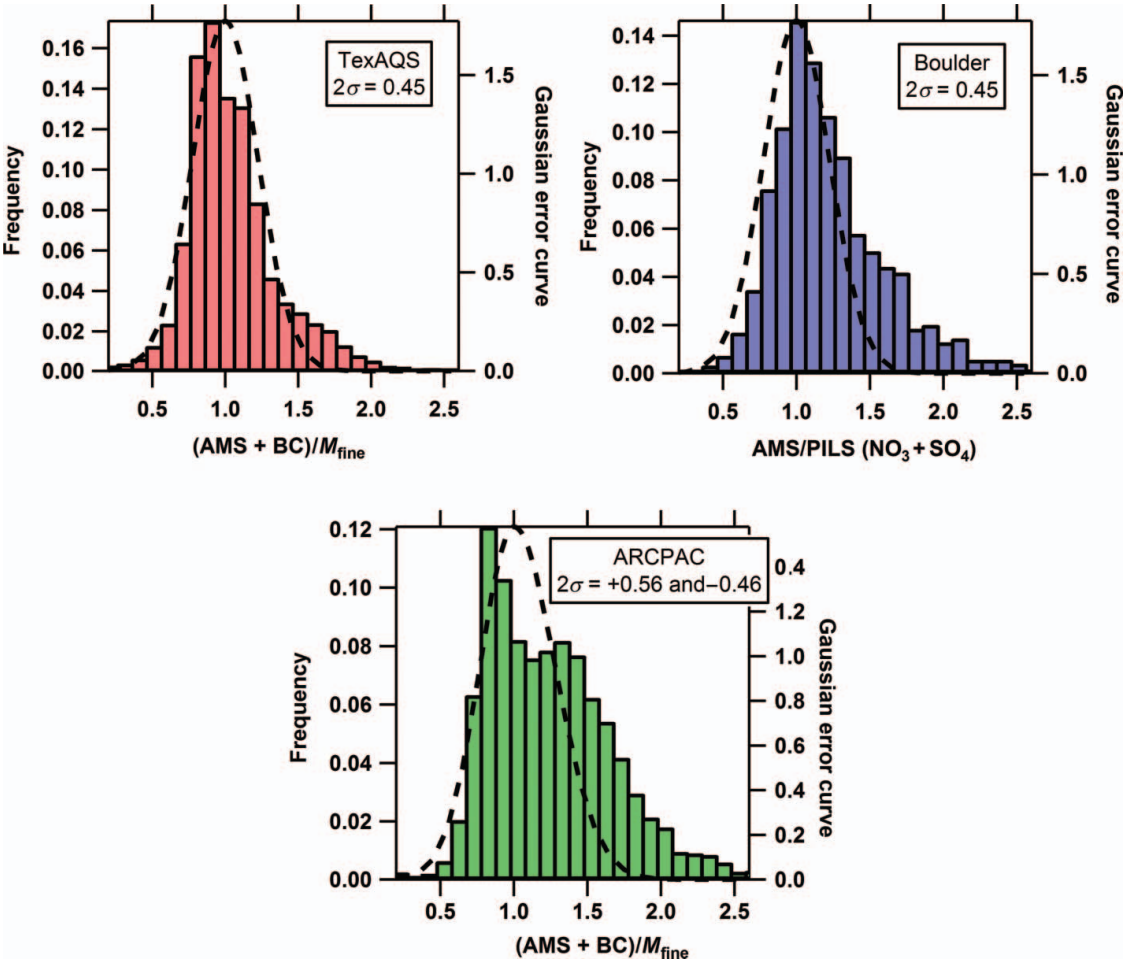

FIG. 1. The frequency distributions of mass ratios from multiple, carefully-operated instruments from the 3 field studies when the default collection efficiency (*CE*) of 0.5 is used for the AMS data. Also plotted are the Gaussian error curves (dashed curves) for the combined measurement uncertainties. Mass ratios that are significantly greater than 1 are likely due to the various effects on the AMS*CE*. (Color figure available online.)

Parameterization of *CE* from Composition

Previous laboratory and field studies have shown clear trends of increasing AMS *CE* with particle acidity, nitrate content, sampling relative humidity, and coatings of pure liquid organic material. Figures 2–4 show a comparison of these various parameterizations of *CE* as a function of aerosol chemical composition. These composition-dependent parameterizations are evaluated using data from the 3 field studies and an algorithm for calculating mass concentrations from these parameterizations is developed.

TABLE 1
Average mass ratios of either AMS + BC to fine particle mass or AMS (nitrate + sulfate) to PILS (nitrate + sulfate) ± 2 standard deviations and the fraction of data that lies within the 2σ combined measurement uncertainties, as indicated for each study, using different *CE* values

		CE = 0.5		*CE* algorithm	
Field study	2σ uncertainties (%)	Ratio	Fraction (%)	Ratio	Fraction (%)
TexAQS: all	45	1.0 ± 1.8	88	0.94 ± 0.62	92
TexAQS: October 5, 2006	45	1.14 ± 0.48	90	0.98 ± 0.28	99.5
Boulder	45	1.17 ± 0.78	81	0.97 ± 0.48	95
ARCPAC	+56 and −46	1.1 ± 3.4	82	0.99 ± 0.64	92

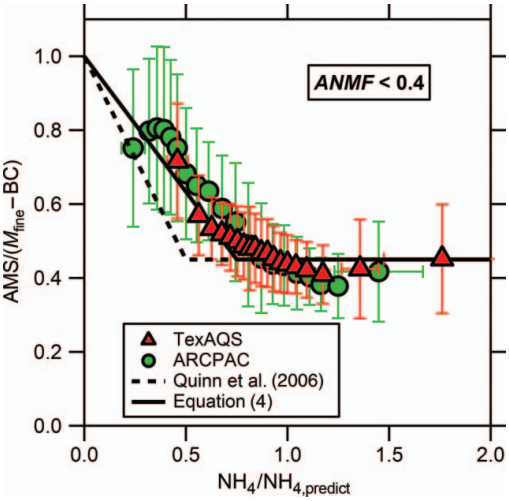

FIG. 2. The ratio of AMS mass to the mass of fine particles (M_{fine}) minus the black carbon (BC) mass (from multiple, carefully-operated instruments) demonstrates the acidity effect, where the apparent *CE* increases for acidic particles (here as a function of the ratio of measured ammonium to predicted ammonium, $NH_4/NH_{4,\text{predict}}$). Error bars are the standard deviations of the averages. Data where the particles have high nitrate content ($ANMF \geq 0.4$), which mainly affected the Boulder dataset, are omitted for clarity. The parameterization from Quinn et al. (2006) field data is shown as the dashed line and Equation 4 is the solid line. (Color figure available online.)

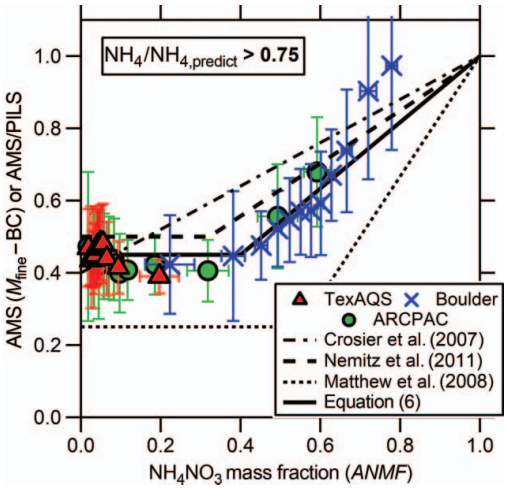

FIG. 3. The ratio of AMS mass to either the mass of fine particles (M_{fine}) minus the black carbon (BC) mass or the PILS-IC mass (from multiple, carefully-operated instruments) demonstrates the nitrate effect, where *CE* increases with nitrate content (here, as a function of ammonium nitrate mass fraction, *ANMF*). Error bars are the standard deviations of the averages. Data where the particles have high acidic content ($NH_4/NH_{4,\text{predict}} \leq 0.75$) are omitted for clarity. The parameterizations described by Crosier et al. (2007), Nemitz et al. (2011), and Matthew et al. (2008) are shown as the dot-dash, dashed, and dotted lines, respectively. Note that the *ANMF*-axis for the Crosier et al. parameterization from field data (based solely on nitrate and sulfate mass) is not precisely the same as for the other field data which included chloride and organic content. Also the particles for the laboratory data parameterized by Matthew et al. did not contain chloride or organic material. Equation 6 is shown as the solid line. (Color figure available online.)

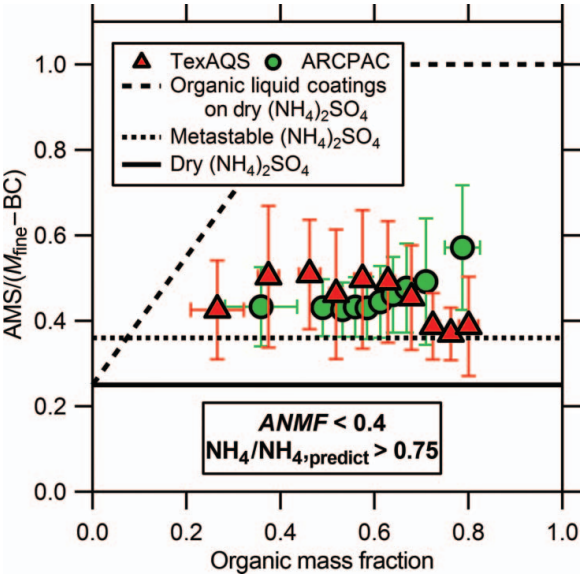

FIG. 4. The ratio of AMS mass to the mass of fine particles (M_{fine}) minus the black carbon (BC) mass (from multiple, carefully-operated instruments) demonstrates the *CE* does not change significantly with organic content. These data were filtered for dry, neutralized, sulfate-rich particles ($NH_4/NH_{4,\text{predict}} > 0.75$ and $ANMF < 0.4$), which removed most of the Boulder data. Error bars are the standard deviations of the averages. The overall average of all these data points (a total of 12989 from the 2 field studies) is 0.45 ± 0.22 (2σ). The *CEs* determined from laboratory experiments by Matthew and coworkers (Matthew et al. 2008) for organic liquid coatings on dry ammonium sulfate, pure, metastable ammonium sulfate, and pure, dry ammonium sulfate are shown as the dashed, dotted, and solid lines respectively. Note there is not any organic material in the uncoated metastable and dry particles (dotted and solid lines). The TexAQS organic material is representative of aged urban organic aerosol (Bahreini et al. 2009) and the ARCPAC organic material is representative of aged biomass burning aerosol (Warneke et al. 2009). (Color figure available online.)

The 3 datasets used in this work exemplify different regimes of the $H^+/NH_4^+/SO_4^{2-}/NO_3^-$ phase diagram, organic mass fraction content, and sampling line *RH* (Figures S1–S3). However, the *RH* in the AMS sampling inlet was greater than 80% only for the Boulder study and these data were also high in ammonium nitrate content. Unfortunately, the effect of *RH* on the *CE* could not be explored independently for these studies. The data presented here were thus restricted to those where the sampling line *RH* was less than 80%.

In order to demonstrate the various effects (acidity, nitrate, and organic) on the AMS *CE*, ambient AMS mass concentrations from all 3 field studies were calculated with a $CE = 1$ and then compared with those obtained from other measurements. Figures 2–4 show the ratio of AMS total (or nitrate + sulfate) mass ($CE = 1$) to total (or nitrate + sulfate) mass from other measurements plotted against parameters representing acidity, nitrate content, and organic content. Note that these measurements were obtained with carefully-operated instruments and took into account variations in particle sampling sizes and

sampling conditions. The data were filtered for all mass concentrations more than 3 times the detection limit and for less humid conditions (sampling line $RH < 80\%$). The mass ratios in Figures 2–4 can be taken as estimates of the AMS *CE* or apparent *CE*, assuming that all other effects have been properly taken into account since AMS mass is now compared with the corresponding mass (i.e., total – BC or nitrate + sulfate) from other measurements.

Effect of High Aerosol Acidity

Figure 2 shows the effect of aerosol acidity on the observed mass ratio. For clarity, periods with high nitrate content (especially observed with the Boulder data) were omitted. If included in this figure, these data points would cluster around $NH_4/NH_{4,predict} = 1.0$ and show a large range of observed mass ratios due to the effect of nitrate content. The nitrate effect is presented in more detail in the discussion below. The level of particle acidity in the datasets is characterized by the ratio between measured ammonium concentration (NH_4) and the theoretically predicted concentration of ammonium ($NH_{4,predict}$) needed to neutralize the inorganic anion mass concentrations observed by the AMS:

$$NH_{4,predict} = 18 \times (SO_4/96 \times 2 + NO_3/62 + Chl/35.45) \quad [3]$$

where SO_4, NO_3, and Chl were the measured aerosol sulfate, nitrate, and chloride mass concentrations (in $\mu g\ m^{-3}$), respectively, from Equation (2) with $CE = 1$ for all species. The ratio $NH_4/NH_{4,predict}$ is correlated with other parameters used to represent acidity such as pH (Zhang et al. 2007b). The AMS-measured chloride is typically dominated by ammonium chloride and not sodium chloride (e.g., Salcedo et al., 2006). Note that this calculation neglected the possibility of ammonium being needed to neutralize organic acids, that a small fraction of the sulfate and nitrate may be due to organosulfates and organonitrates (Farmer et al. 2010), and assumes the particles are internally-mixed with the same *CE*.

In field measurements Quinn and coworkers observed that if sulfate was fully or partially acidic, the *CE* increased linearly to 1 with increasing acidity (Quinn et al. 2006). For partially or fully neutralized particles, the *CE* was 0.45. While the typical default *CE* is 10% higher than this, the difference is small considering the 30% uncertainty determined for *CE* (Bahreini et al. 2009). The equation for *CE* used in the Quinn et al. work was converted into a function of $NH_4/NH_{4,predict}$ for Figure 2 as: $CE = \max[0.45, 1.0–1.1 \times (NH_4/NH_{4,predict})]$. As shown below and in Figure 4, the average for ambient ammonium sulfate particles is 0.45 ± 0.22 (2σ), hence 0.45 was considered a lower limit on the *CE* of ambient particles. Although the field data in Figure 2 agree with the previously published parameterization of Quinn et al. when considering the observed variability as represented by the error bars, the averaged dry *CE* appears to be more closely represented by:

$$CE_{dry} = \max\left(0.45, 1.0 - 0.73 \times \left({}^{NH_4}/_{NH_{4,predict}}\right)\right) \quad [4]$$

One potential explanation for this slight difference is that the mass from fine particle volume shown in Figure 2 was corrected for AMS lens transmission efficiency whereas the Quinn et al. parameterization was based on the AMS sulfate mass compared with PILS-IC sulfate mass and may not have accounted for differences in particle transmission between the 2 instruments.

Effect of High Ammonium Nitrate Fraction

Figure 3 shows the variation in mass ratio as a function of nitrate content in the sampled aerosol for the 3 studies. For simplification periods where the acidity effect discussed above is active are removed and only the data where particles were mostly neutralized are shown. Here the aerosol nitrate content is characterized by the ammonium nitrate mass fraction (*ANMF*) as follows:

$$ANMF = \frac{80/62 \times NO_3}{(NH_4 + SO_4 + NO_3 + Chl + Org)} \quad [5]$$

where NH_4, SO_4, NO_3, Chl, and Org were the measured aerosol ammonium, sulfate, nitrate, chloride, and organic concentrations (in $\mu g\ m^{-3}$), respectively, from Equation (2) with $CE = 1$ for all species. Again, this assumes that the particles are internally mixed and have the same *CE*.

Previous laboratory and field work both yielded $CE = 1$ for $ANMF = 1$ (Jayne et al. 2000; Crosier et al. 2007; Matthew et al. 2008; Nemitz et al. 2011). Yet, the previous work differed in the *CE* for $ANMF = 0$ and how the *CE* increased with *ANMF*. The *CE* parameterizations from previous work are shown in Figure 3. For this representation, the Crosier et al. parameterization from field data which only included nitrate and sulfate mass was converted into a function of *ANMF* neglecting the chloride and organic concentrations: $CE = 0.393 + 0.582 \times ANMF$. Note that the *ANMF*-axis depicted in Figure 3 for their parameterization (based solely on nitrate and sulfate mass) is not precisely the same as for the other curves which included chloride and organic content. For pure, dry mixed ammonium sulfate/ammonium nitrate particles with an *ANMF* less than 0.55, the laboratory *CE* was similar to that of pure, dry ammonium sulfate where $CE = 0.24$ and fairly constant (Matthew et al. 2008). Above $ANMF = 0.55$, the laboratory *CE* increased linearly with *ANMF*. For the field data reported by Crosier and coworkers (2007), the *CE* increased linearly from 0.4 for ammonium sulfate ($ANMF = 0$) to 1 for ammonium nitrate ($ANMF = 1$). The Nemitz et al. parameterization is from the EUCAARI (European Integrated Project on Aerosol Cloud Climate Air Quality Interactions) field project and is between the 2 other parameterizations (Nemitz et al. 2011). The data reported here when taken together with the previous field and laboratory studies suggest a different

ANMF-dependent *CE* parameterization as follows:

$$CE_{\text{dry}} = \max(0.45, 0.0833 + 0.9167 \times ANMF) \quad [6]$$

in which a constant *CE* of 0.45 is used for $ANMF \leq 0.4$ and a linear *CE* increase up to 1 for $ANMF > 0.4$. The *ANMF* where the *CE* increases in this parameterization (0.4) is a bit lower than it is for pure, laboratory particles (0.55), perhaps due to the effect of organic material in ambient particles.

Lack of Effect of High Organic Fraction

In the atmosphere, inorganic aerosol constituents such as sulfate and nitrate are internally mixed with organic aerosol material (Murphy et al. 2006; Zhang et al. 2007a). Laboratory studies have shown an effect of the organic content on the AMS *CE* when the organic material is a liquid coating on solid ammonium sulfate (Matthew et al. 2008). In that work, the *CE* linearly increased from the dry value up to 1 for an organic mass fraction of approximately 50%. Whether or not the organic content has an effect on the *CE* for ambient particles is explored here with data from 2 field studies, where Figure 4 shows the observed mass ratios as a function of organic aerosol mass fraction for aerosols with dominantly an inorganic composition of ammonium sulfate. Data points with high nitrate content (especially observed with the Boulder data) were excluded from this figure because the nitrate effect would obscure an organic effect on *CE*. This figure indicates that changes in organic content between 25 and 80% do not have a clear effect on AMS *CE*. The lack of a strong organic effect in the AMS *CE* may be consistent with recent findings that ambient organic aerosols are solids and not liquids at low relative humidities (Virtanen et al. 2010), which are present in the AMS inlet. Furthermore, the aged urban aerosol (TexAQS) and the aged biomass burning aerosols (ARCPAC) behaved similarly, which suggests that these types of organic aerosol are probably not liquid when detected by the AMS instrument. The overall average of all 12989 data points from the 2 field studies is 0.45 ± 0.22 (2σ). Note that this error bar represents the combined uncertainty of both the AMS and UHSAS. These results need to be tested further with fresh organic aerosols.

While laboratory measurements have shown a *CE* of approximately 0.25 for pure, dry ammonium sulfate (Matthew et al. 2008), most ambient internally mixed sulfate/organic particles, however, display a higher *CE* around 0.45 (Figure 4). In the relative humidity range of 32–80% *RH* for dehydrating particles, pure ammonium sulfate particles are metastable liquids in the atmosphere and have a statistically higher *CE* of 0.36 versus 0.25 for dry particles (Matthew et al. 2008). Yet the *CE* for the metastable particles is also on average lower than the *CE* for the ambient particles (Figure 4). Thus, it is possible that the ubiquitous organic content plays a role in increasing the *CE* of ammonium sulfate to about 0.45 in internally mixed particles.

Effect of High RH

Because only the Boulder data had points when the sampling line *RH* was greater than 80% and these points were also high in *ANMF*, the effect of *RH* on the *CE* could not be independently investigated for these studies. However, an *RH* effect was observed in an ambient data set obtained at Trinidad Head, CA, where the mass concentrations of sulfate increased by a factor of about 2 when the *RH* was higher than 71% (Allan et al. 2004a). Here, an *RH*-dependent parameterization of *CE* was estimated based on the laboratory work by Matthew et al. (2008). Since particles lose water to some extent in the AMS lens and vacuum chamber, the sampling line *RH* where particles solidify in the AMS was typically higher than the crystallization *RH* and where particles become liquid was approximately equal to the deliquescence *RH* (Matthew et al. 2008). Matthew and coworkers showed that if the sampling line *RH* falls between 80 and 90%, the *CE* increased linearly from the "dry" *CE*. The observed relationship can be summarized as follows:

$$CE = \max(CE_{\text{dry}}, (5 \times CE_{\text{dry}} - 4) + (1 - CE_{\text{dry}})/20 \times RH) \quad [7]$$

where CE_{dry} was the *CE* based on the dry particle composition from either Equation 4 or 6 above and *RH* refers to the relative humidity of the sampling inlet line (in %). If *RH* was not measured or was less than 80%, *CE* was set to CE_{dry}. Again, this estimation was approximate and did not take metastable phases into account, other than ammonium nitrate. Additional studies

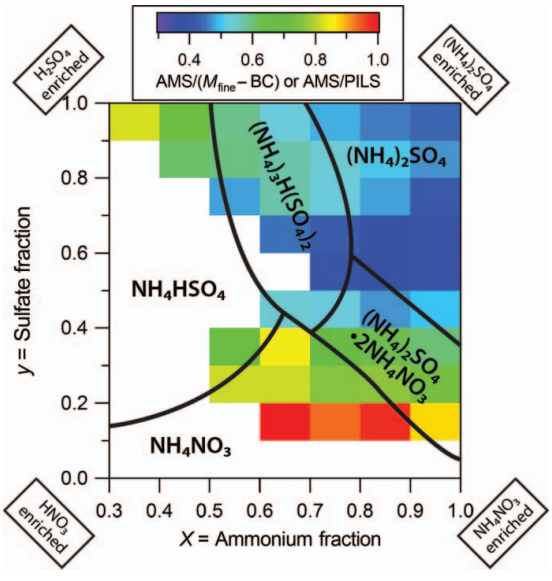

FIG. 5. The Comparison of the apparent *CE* (from the ratio of measurements from multiple, carefully-operated instruments) from all 3 field studies with the dry phase diagram for the $H^+/NH_4^+/SO_4^{2-}/NO_3^-$ system at 298 K (Martin 2000). Note that the calculation of cation mole fraction (X) and anion mole fraction (Y) only included the species H^+, ammonium, sulfate, and nitrate for the field data and did not include chloride or organic content.

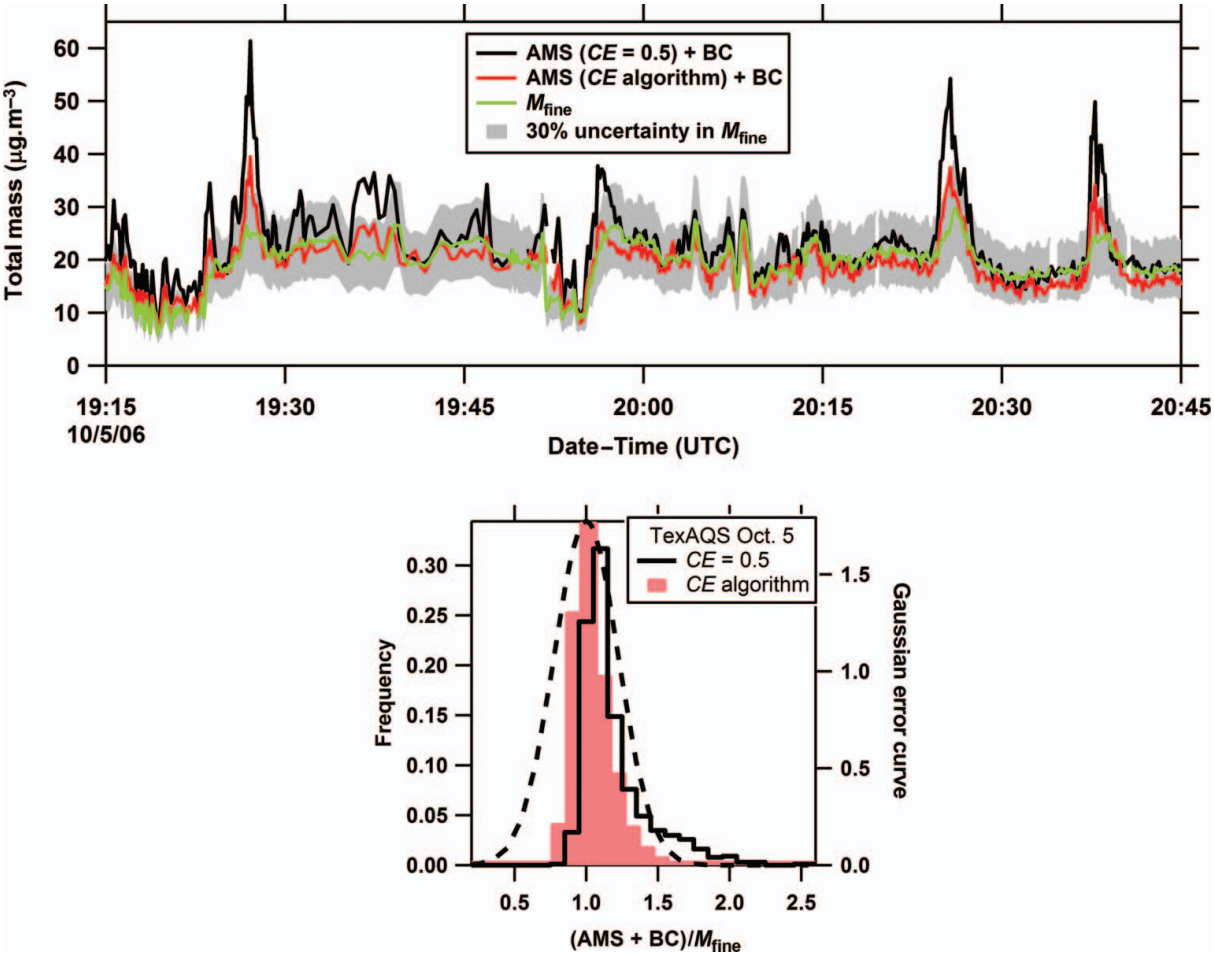

FIG. 6. Example of the acidity effect showing a portion of flight data from October 5, 2005 around Houston with the AMS $CE = 0.5$ (solid, black curve) or with *CE* as a function of the composition-dependent algorithm. The calculated fine particle mass (M_{fine}) is shown in the top panel with the AMS plus black carbon (BC) mass and the frequency distributions of the ratio of the AMS total mass from the 2 *CEs* plus BC mass to M_{fine} for the entire flight are shown in the bottom panel. The gray region (top panel) shows ± 30% (2σ) uncertainty in fine particle volume measurements and the dashed curve (bottom panel) is the Gaussian error curve with the 2σ combined measurement uncertainty (45%). (Color figure available online.)

are needed to assess the *RH* parameterization of *CE* shown in Equation 7.

A representation of the effect of acidity and nitrate content on the apparent *CE* is shown in Figure 5 with the isothermal phase diagram for the $H^+/NH_4^+/SO_4^{2-}/NO_3^-$ system at dry conditions (Martin 2000). In general, the apparent *CE* is broadly consistent with known solid/liquid phases at 298 K. Variability is likely due to drying in the AMS instrument and the relatively wide range of sampling temperatures for the AMS (from 267 to 310 K for the 3 studies). Note that in addition to ionic composition, relative humidity, and temperature, the phase of atmospheric particles may also depend on the organic content or the presence of inclusions to promote efflorescence of metastable phases such as ammonium nitrate.

Algorithm Including All Effects

An algorithm was developed to estimate the chemical composition-dependent *CE* according to the parameterizations shown in Equations (4) and (6) for the 3 datasets (see supplemental information for the Igor procedure file). There were 2 main steps to this algorithm. In the first step, the *CE* was estimated with Equations (4) or (6). It is useful to note that the *CE* corrections for nitrate content and particle acidity in these equations do not conflict with each other since ammonium nitrate forms under conditions when ammonium sulfate is partially or fully neutralized at tropospheric temperatures (Wexler and Clegg 2002). This is clear for the ARCPAC data set which spanned the 2 extremes, acidic and high nitrate content particles, during various times in the field study (Figures 2, 3, and S3). Second, if the

data contained points where the sampling line *RH* was greater than 80%, these "dry" *CEs* would have been adjusted using Equation (7). Because the data here were restricted to $RH < 80\%$, the *CE* calculated only from step 1 was used. The particle composition was assumed to be internally mixed and *CE* from the algorithm was applied to all species equally for each data point.

Using this approach, the *CE* was estimated for each AMS measurement point in time and might introduce errors due to the noise in the reported mass concentrations as a function of time. Here, because most of the data were obtained from an airborne platform and often varied significantly on short time scales, we smoothed the measured species in the time series by at most 1 point (or 2 points for ammonium) and averaged the aerosol mass distributions in the plumes whenever a size-dependent *CE* was needed. Such time smoothing is recommended for future studies when it helps reduce the effect of noise on the estimated *CE*.

CASE STUDIES

As shown in Figures 2–4 and Figures S1–S3, TexAQS represents a study with pollution events that are acidic, Boulder has variable and sometimes high nitrate content, and ARCPAC contains measurements with high nitrate content from a flight above Colorado, has some acidic aerosol over Alaska, and serves a test case to evaluate the effect of variable amounts of organic material. In this work, the default *CE* is used to obtain base-case mass concentrations (Figure 1). The base-case mass concentrations are then compared with mass concentrations that are calculated with variable *CE* values that are obtained from composition-dependent algorithm using Equations 4 and 6.

Case 1: TexAQS-II, Summer/Fall 2006

Airborne measurements of aerosol chemical composition were obtained as part of the Texas Air Quality Study/Gulf of Mexico Atmospheric Composition and Climate Study (TexAQS-II/GoMACCS) to understand air pollution around eastern Texas (Bahreini et al. 2009). As shown in Figure 1 and Table 1, 88% of the TexAQS data was within the experimental uncertainties using the default *CE* of 0.5. Here, we discuss an example of a specific flight where use of the default *CE* was inappropriate.

For the flight of October 5, 2005, the average acidity was higher than it was for most of the field study (Figure S1). The top panel of Figure 6 focuses on a short time period of this flight and shows the total mass from the AMS using $CE = 0.5$ and also using the algorithm, mainly the acidity correction of Equation (4), plus BC mass. The calculated mass from fine particle volume (M_{fine}) is also shown on this trace with its 30% (2σ) uncertainty. Several points in the speciated mass from the AMS with the default *CE* plus BC lie above this uncertainty band, suggesting that the AMS mass calculated using $CE = 0.5$ is too high. The distribution of the ratio of the speciated total mass to the fine particle mass for the entire flight is shown in the bottom panel. Note that when the *CE* algorithm is used, the distribution in data points for this flight is much narrower than the Gaussian distribution of random errors, demonstrating that in some cases the particles are more homogeneous and the variability in *CE* is less than 30%.

Using the default *CE*, 90% of the AMS + BC data points were within the experimental uncertainties (Table 1). When the algorithm with the acidity correction to the AMS *CE* was applied instead of the default *CE*, this fraction increased to 99%. For this flight, the average ratio of the speciated mass to the fine particle mass with the corrected *CE* was 0.98 ± 0.28 (2 standard

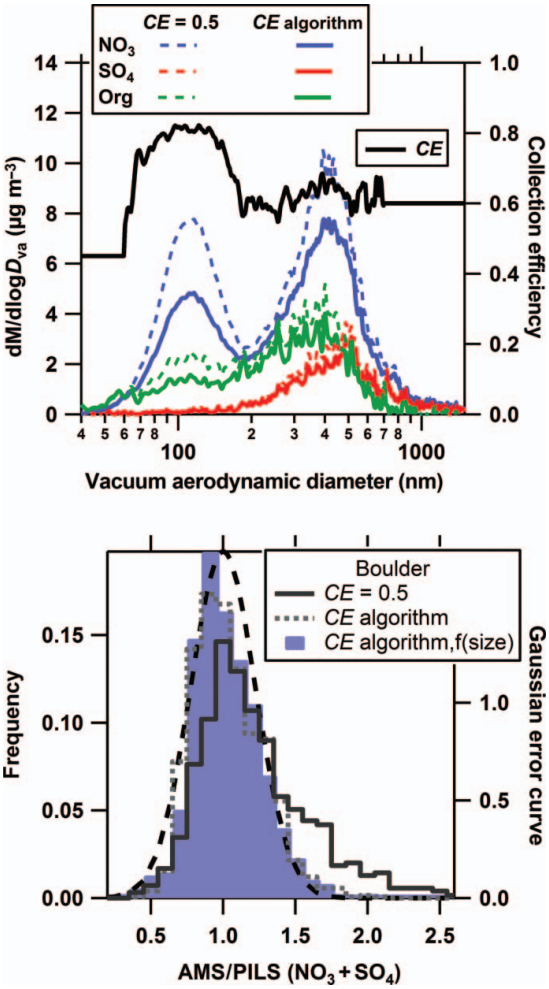

FIG. 7. Mass concentrations as a function of vacuum aerodynamic diameter (d_{va}) for various species measured with the AMS at Boulder, CO from 18:02 MST on February 6, 2005 to 02:02 MST on February 7, 2005 (top panel). The mass concentrations for each species were calculated using the collection efficiencies using $CE = 0.5$ for all species (dashed curves) and then using the composition- and size-resolved *CE* algorithm (solid curves). The bottom panel shows the frequency distributions of the ratio of the AMS to PILS mass for nitrate plus sulfate mass using the default *CE*, the composition-dependent *CE* algorithm, and the full composition- and size-dependent *CE* algorithm for the entire field study. The dashed curve (bottom panel) is the Gaussian error curve with the 2σ combined measurement uncertainty (45%).

deviations), whereas it was 1.14 ± 0.48 (2 standard deviations) with the default *CE* (Table 1).

Case 2: Boulder, CO, Winter 2005

We applied the *CE* algorithm to an AMS data set collected during a ground-based study from January 26 to February 9, 2005 at a mesa site overlooking the southwestern edge of Boulder. For most of the study, aerosol sulfate was primarily in the accumulation mode and aerosol nitrate, ammonium, and organic material were distributed in the accumulation mode as well as in a smaller mode (Figure S4). Because the AMS lens transmission efficiency was 100% for particles between 100 and 560 nm and there were times when a mode of smaller particles was present, the *CE* algorithm was mainly evaluated for the time periods where this small mode was not present (i.e., nitrate present in the small mode was contributing to <40% of the total nitrate). For these time periods, a large fraction of the ambient submicron mass was measured by the AMS and the particles measured by the AMS were likely measured by the bulk PILS-IC. There was sufficient ammonium to fully neutralize both the sulfate and nitrate (slope of measured to predicted $NH_4 = 0.93$, $r^2 = 0.88$) and the *ANMF* was often more than 60% across the size range with most of the mass (Figure S4). Hence, a composition-dependent *CE* is likely to help improve the ratio of AMS nitrate plus sulfate mass to the PILS nitrate plus sulfate mass calculated using the default *CE* (Figure 1). While the higher nitrate content affects the overall applicability of $CE = 0.5$ for this dataset, the lack of a strong size-dependence on the *ANMF* on average suggests that applying a size-dependent *CE* might not be important for this dataset.

There were, however, time periods where the *ANMF* varied across the size range measured. An example of this is shown in Figure 7. Here the ammonium nitrate mass fraction was higher in the smaller mode than in the larger mode, making the estimated *CE* change as a function of size. Applying the composition-dependent *CE* algorithm as a function of size results in a slightly different shape to the mass distributions since the *CE* was higher for the smaller particles where there was relatively more ammonium nitrate. Unfortunately, high-quality, dry volume distribution data are not available for this field study, which would allow a direct evaluation of the composition- and size-dependent *CE*.

For this dataset, mass distributions were obtained every 2.5 min and typically had sufficient signal-to-noise to generate a *CE* from the algorithm using the mass distributions as a function of time. This composition- and size-dependent *CE* was then applied across each of the species in individual mass distributions, which were integrated to give the final mass concentrations for each species. Using the default *CE*, 81% of the mass ratios of AMS to PILS data were within the experimental uncertainties (Table 1). When the algorithm with the nitrate-content correction to the AMS *CE* was applied instead of the default *CE*, this fraction increased to 95%. For both the bulk and size-dependent *CEs* from the algorithm, less than 3% of data points with mass ratios greater than 1 were outside the maximum range of uncertainties from random effects whereas for the default *CE* this fraction was 18%. The final mass ratios of AMS to PILS data improved from 1.17 ± 0.78 (2 standard deviations) using the default *CE* to 0.97 ± 0.48 (2 standard deviations) for the *CE* as a function of both composition and size (Figure 7 and Table 1). While applying only the composition-dependent *CE* algorithm to the entire field study improves the mass ratios of the AMS to PILS for nitrate plus sulfate and follows the Gaussian distribution of random errors from the combined measurement uncertainties, using the composition- and size-dependent *CE* narrows the distribution of data points further.

Case 3: ARCPAC, Spring 2008

For the ARCPAC study, 18% of the data points had mass ratios beyond the combined uncertainties when $CE = 0.5$ was used (Figure 1), when less than 5% were expected due to random effects. This case was the only 1 of the 3 studies where both compositional extremes were observed: high acidity (Figure 2) and high nitrate content (Figure 3). Furthermore, the particle composition during the latter part of this field study was dominated by organic material from aged biomass burning particles, which had been transported to the Arctic from fires in Siberia and Kazakhstan (Warneke et al. 2009). The BC mass fraction for the entire field study including the biomass burning particles was less than 5%. When the composition-dependent *CE* was applied, the mass concentrations for the acidic and nitrate-dominated points were reduced and 13% more of the mass ratios were closer to 1.0 and within the uncertainties (Figure 8). The distribution created using the *CE* algorithm for the AMS mass clearly fits the Gaussian distribution of random errors more closely than that created using the default *CE*. The average mass ratio and its standard deviation improved from 1.1 ± 1.7 (2

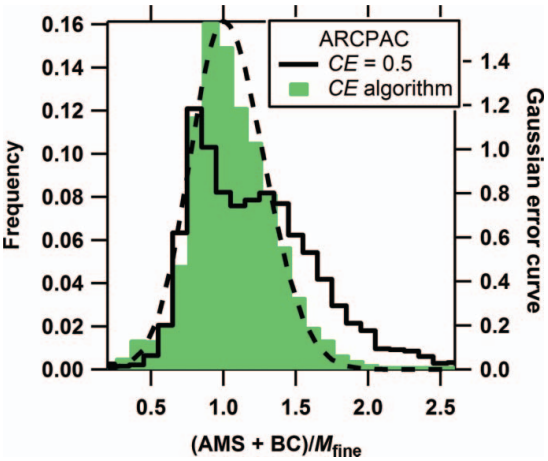

FIG. 8. Ratio of the AMS plus black carbon (BC) mass to the fine particle mass (M_{fine}) for the entire ARCPAC study using either the default *CE* or the *CE* algorithm. The dashed curve is the Gaussian error curve with the 2σ combined measurement uncertainty (+56/–46%). (Color figure available online.)

TABLE 2
Results from orthogonal distance regressions with an intercept through zero of the total measured mass, either from AMS + BC versus fine particle mass, or AMS (nitrate + sulfate) versus PILS (nitrate + sulfate) for each study using different *CE* values (shown in Figures S5–S8)

		$CE = 0.5$			*CE* algorithm		
Field study	Number of data points	slope	R^2	χ^2	slope	R^2	χ^2
TexAQS: all	13275	0.98	0.82	68509	0.96	0.90	29835
TexAQS: October 5, 2006	1543	1.15	0.72	10289	0.98	0.85	3699
Boulder	1228	1.23	0.80	3048	0.96	0.92	914
ARCPAC	2622	0.86	0.92	12827	0.89	0.95	8716

standard deviations) using the default *CE* to 0.99 ± 0.32 (2 standard deviations) using the composition-dependent *CE* algorithm.

CONCLUSIONS

An algorithm was created for estimating AMS *CE* for field data based on the aerosol chemical composition and sampling line *RH* in addition to laboratory and field measurements of *CE*. This approach improves quantification of AMS mass concentrations in comparison with other particle mass measurements in cases where particles are acidic or contain large amounts of nitrate, where the *CE* is actually higher than the default *CE* of 0.5. It is useful to note that for all 3 datasets particles that are not acidic and do not contain large amounts of nitrate have a base *CE* of 0.45. The default *CE* of 0.5 that has been typically used in ambient AMS measurements lies within the uncertainty of this value. In the datasets where the algorithm was applied, particle composition sometimes varied across different size ranges and a composition-dependent *CE* as a function of size was needed to achieve better agreement with other particle measurements. Consistent with previous results, in the base case scenario in which $CE = 0.5$ is used for all data points, the agreement between AMS mass and external measurements of mass lies within the experimental uncertainties for at least 81% of the data. In all case studies, the systematic positive biases in the mass ratios were indicative of the need for a higher *CE* than the default. For these situations, the mass concentrations using the default *CE* may be too high by as much as a factor of 2. In the field studies examined here, the mass concentrations using the *CE* algorithm compared with using the default *CE* decreased on average by 6% (TEXAQS), 16% (Boulder), and 10% (ARCPAC). The departures from the default *CE* allow for better descriptions of individual events and may be particularly necessary for environments with high acidity, nitrate content, and/or sampling inlet *RH*. Tables 1 and 2 summarize how the algorithm improved the mass ratio for all 3 studies, reducing the systematic positive biases depicted in Figure 1 and increasing the linear correlation between the various methods of determining submicron aerosol mass. Furthermore, when the *CE* algorithm was applied, these data points fell into the range of data expected by random error of the combined measurement uncertainties with a 30% (2σ) uncertainty in AMS mass concentration. The variability in organic content does not seem to correlate with obvious changes in *CE* across the 3 environments. Due to the potential additional variation of *CE* at high humidity levels (Allan et al. 2004a; Ng et al. 2011), it is recommended that the AMS sampling line be dried to low humidities (∼20% RH) before entering the AMS. This strategy simplifies the application of the composition-dependent *CE* determined in this paper and reduces further losses for particles that become too large to be transmitted through the lens when hydrated. Although the application of this algorithm appears to provide reasonable AMS mass concentrations for these field data sets, it should be tested with other data sets, especially to determine effect of sampling line *RH* and different organic materials in a variety of environments.

REFERENCES

Aiken, A. C., Salcedo, D., Cubison, M. J., Huffman, J. A., DeCarlo, P. F., Ulbrich, I. M., et al. (2009). Mexico City Aerosol Analysis During MILAGRO Using High Resolution Aerosol Mass Spectrometry at the Urban Supersite (T0). Part 1: Fine Particle Composition and Organic Source Apportionment. *Atmos. Chem. Phys.* 9:6633–6653, doi:10.5194/acp-9–6633-2009.

Alfarra, M. R., Coe, H., Allan, J. D., Bower, K. N., Boudries, H., Canagaratna, M. R., et al. (2004). Characterization of Urban and Rural Organic Particulate in the Lower Fraser Valley Using Two Aerodyne Aerosol Mass Spectrometers. *Atmos. Environ.* 38:5745–5758, doi:10.1016/j.atmosenv.2004.01.054.

Allan, J. D., Alfarra, M. R., Bower, K. N., Williams, P. I., Gallagher, M. W., Jimenez, J. L., et al. (2003a). Quantitative Sampling Using an Aerodyne Aerosol Mass Spectrometer 2. Measurements of Fine Particulate Chemical Composition in Two U.K. Cities. *J. Geophys. Res.* 108:4091, doi:10.1029/2002JD002359.

Allan, J. D., Bower, K. N., Coe, H., Boudries, H., Jayne, J. T., Canagaratna, M. R., et al. (2004a). Submicron Aerosol Composition at Trinidad Head, California, During ITCT 2K2: Its Relationship with Gas Phase Volatile Organic Carbon and Assessment of Instrument Performance. *J. Geophys. Res.* 109:D23S24, doi:10.1029/2003JD004208.

Allan, J. D., Delia, A. E., Coe, H., Bower, K. N., Alfarra, M. R., Jimenez, J. L., et al. (2004b). A Generalised Method for the Extraction of Chemically Resolved Mass Spectra from Aerodyne Aerosol Mass Spectrometer Data. *J. Aerosol Sci.* 35:909–922, doi:10.1016/j.jaerosci.2004.02.007.

Allan, J. D., Jimenez, J. L., Williams, P. I., Alfarra, M. R., Bower, K. N., Jayne, J. T., et al. (2003b). Quantitative Sampling Using an Aerodyne Aerosol Mass Spectrometer 1. Techniques of Data Interpretation and Error Analysis. *J. Geophys. Res.* 108:4090, doi:10.1029/2002JD002358.

Asa-Awuku, A., Moore, R. H., Nenes, A., Bahreini, R., Holloway, J. S., Brock, C. A., et al. (2011). Airborne Cloud Condensation Nuclei Measurements During the 2006 Texas Air Quality Study. *J. Geophys. Res.* 116:D11201, doi:10.1029/2010JD014874.

Bahreini, R., Dunlea, E. J., Matthew, B. M., Simons, C., Docherty, K. S., DeCarlo, P. F., et al. (2008). Design and Operation of a Pressure-Controlled Inlet for Airborne Sampling with an Aerodynamic Aerosol Lens. *Aerosol Sci. Technol.* 42:465–471, doi:10.1080/02786820802178514.

Bahreini, R., Ervens, B., Middlebrook, A. M., Warneke, C., de Gouw, J. A., DeCarlo, P. F., et al. (2009). Organic Aerosol Formation in Urban and Industrial Plumes Near Houston and Dallas, Texas. *J. Geophys. Res.* 114:D00F16, doi:10.1029/2008JD011493.

Brock, C. A., Cozic, J., Bahreini, R., Froyd, K. D., Middlebrook, A. M., McComiskey, A., et al. (2011). Characteristics, Sources, and Transport of Aerosols Measured in Spring 2008 During the Aerosol, Radiation, and Cloud Processes Affecting Arctic Climate (ARCPAC) Project. *Atmos. Chem. Phys.* 11:2423–2453, doi:10.5194/acp-11-2423-2011.

Canagaratna, M. R., Jayne, J. T., Jimenez, J. L., Allan, J. D., Alfarra, M. R., Zhang, Q., et al. (2007). Chemical and Microphysical Characterization of Ambient Aerosols with the Aerodyne Aerosol Mass Spectrometer. *Mass Spectrom. Rev.* 26:185–222, doi:10.1002/mas.20115.

Cappa, C. D., and Jimenez, J. L. (2010). Quantitative Estimates of the Volatility of Ambient Organic Aerosol. *Atmos. Chem. Phys.* 10:5409–5424, doi:10.5194/acp-10-5409-2010.

Crosier, J., Allan, J. D., Coe, H., Bower, K. N., Formenti, P., and Williams, P. I. (2007). Chemical Composition of Summertime Aerosol in the Po Valley (Italy), Northern Adriatic and Black Sea. *Q. J. Roy. Meteor. Soc.* 133:61–75, doi:10.1002/qj.88.

Cross, E. S., Onasch, T. B., Canagaratna, M., Jayne, J. T., Kimmel, J., Yu, X.-Y., et al. (2009). Single Particle Characterization Using a Light Scattering Module Coupled to a Time-of-Flight Aerosol Mass Spectrometer. *Atmos. Chem. Phys.* 9:7769–7793, doi:acp-9-7769-2009.

Cross, E. S., Slowik, J. G., Davidovits, P., Allan, J. D., Worsnop, D. R., Jayne, J. T., et al. (2007). Laboratory and Ambient Particle Density Determinations Using Light Scattering in Conjunction with Aerosol Mass Spectrometry. *Aerosol Sci. Technol.* 41:343–359, doi:10.1080/02786820701199736.

de Gouw, J. A., Brock, C. A., Atlas, E. L., Bates, T. S., Fehsenfeld, F. C., Goldan, P. D., et al. (2008). Sources of Particulate Matter in the Northeastern United States in Summer: 1.Direct Emissions and Secondary Formation of Organic Matter in Urban Plumes. *J. Geophys. Res.* 113:D08301, doi:10.1029/2007JD009243.

de Gouw, J. A., Middlebrook, A. M., Warneke, C., Goldan, P. D., Kuster, W. C., Roberts, J. M., et al. (2005). Budget of Organic Carbon in a Polluted Atmosphere: Results from the New England Air Quality Study in 2002. *J. Geophys. Res.* 110:D16305, doi:10.1029/2004JD005623.

DeCarlo, P. F., Dunlea, E. J., Kimmel, J. R., Aiken, A. C., Sueper, D., Crounse, J., et al. (2008). Fast Airborne Aerosol Size and Chemistry Measurements Above Mexico City and Central Mexico During the MILAGRO Campaign. *Atmos. Chem. Phys.* 8:4027–4048, doi:10.5194/acp-8-4027-2008.

DeCarlo, P. F., Kimmel, J. R., Trimborn, A., Northway, M. J., Jayne, J. T., Aiken, A. C., et al. (2006). Field-Deployable, High-Resolution, Time-of-Flight Aerosol Mass Spectrometer. *Anal. Chem.* 78:8281–8289, doi: 8210.1021/ac061249n.

DeCarlo, P. F., Slowik, J. G., Worsnop, D. R., Davidovits, P., and Jimenez, J. L. (2004). Particle Morphology and Density Characterization by Combined Mobility and Aerodynamic Diameter Measurements. Part 1: Theory. *Aerosol Sci. Technol.* 38:1185–1205, doi:10.1080/027868290903907.

Drewnick, F., Hings, S. S., DeCarlo, P., Jayne, J. T., Gonin, M., Fuhrer, K., et al. (2005). A New Time-of-Flight Aerosol Mass Spectrometer (TOF-AMS) - Instrument Description and First Field Deployment. *Aerosol Sci. Technol.* 39:637–658, doi:10.1080/02786820500182040.

Drewnick, F., Schwab, J. J., Jayne, J. T., Canagaratna, M., Worsnop, D. R., and Demerjian, K. L. (2004). Measurements of Ambient Aerosol Composition During PMTACS-NY 2001 Using an Aerosol Mass Spectrometer. Part I: Mass Concentrations. *Aerosol Sci. Technol.* 38:92–103, doi:10.1080/02786820390229507.

Engelhart, G. J., Hildebrandt, L., Kostenidou, E., Mihalopoulos, N., Donahue, N. M., and Pandis, S. N. (2011). Water Content of Aged Aerosol. *Atmos. Chem. Phys.* 11:911–920, doi:10.5194/acp-11-911-2011.

Farmer, D. K., Matsunaga, A., Docherty, K. S., Surratt, J. D., Seinfeld, J. H., Ziemann, P. J., et al. (2010). Response of an Aerosol Mass Spectrometer to Organonitrates and Organosulfates and Implications for Atmospheric Chemistry. *Proc. Natl. Acad. Sci. U.S.A.* 107:6670–6675, doi:10.1073/pnas.0912340107.

Hogrefe, O., Schwab, J. J., Drewnick, F., Lala, G. G., Peters, S., Demerjian, K. L., et al. (2004). Semicontinuous PM2.5 Sulfate and Nitrate Measurements at an Urban and a Rural Location in New York: PMTACS-NY Summer 2001 and 2002 Campaigns. *J. Air Waste Manage. Assoc.* 54:1040–1060.

Huffman, J. A., Docherty, K. S., Aiken, A. C., Cubison, M. J., Ulbrich, I. M., DeCarlo, P. F., et al. (2009). Chemically-Resolved Aerosol Volatility Measurements from two Megacity Field Studies. *Atmos. Chem. Phys.* 9:7161–7182, doi:10.5194/acp-9-7161-2009.

Huffman, J. A., Jayne, J. T., Drewnick, F., Aiken, A. C., Onasch, T., Worsnop, D. R., et al. (2005). Design, Modeling, Optimization, and Experimental Tests of a Particle Beam Width Probe for the Aerodyne Aerosol Mass Spectrometer. *Aerosol Sci. Technol.* 39:1143–1163, doi:10.1080/02786820500423782.

Jayne, J. T., Leard, D. C., Zhang, X., Davidovits, P., Smith, K. A., Kolb, C. E., et al. (2000). Development of an Aerosol Mass Spectrometer for Size and Composition Analysis of Submicron Particles. *Aerosol Sci. Technol.* 33:49–70, doi:10.1080/027868200410840.

Jimenez, J. L., Canagaratna, M. R., Donahue, N. M., Prevot, A. S. H., Zhang, Q., Kroll, J. H., et al. (2009). Evolution of Organic Aerosols in the Atmosphere. *Science* 326:1525–1529, doi:10.1129/science.1180353.

Jimenez, J. L., Jayne, J. T., Shi, Q., Kolb, C. E., Worsnop, D. R., Yourshaw, I., et al. (2003). Ambient Aerosol Sampling Using the Aerodyne Aerosol Mass Spectrometer. *J. Geophys. Res.* 108:8425, doi:10.1029/2001JD001213.

Khlystov, A., Stanier, C. O., Takahama, S., and Pandis, S. N. (2005). Water Content of Ambient Aerosol During the Pittsburgh Air Quality Study. *J. Geophys. Res.* 110:D07S10, doi:10.1029/2004JD004651.

Kiendler-Scharr, A., Zhang, Q., Hohaus, T., Kleist, E., Mensah, A., Mentel, T. F., et al. (2009). Aerosol Mass Spectrometric Features of Biogenic SOA: Observations from a Plant Chamber and in Rural Atmospheric Environments. *Environ. Sci. Technol.* 43:8166–8172, doi:10.1021/es901420b.

Kleinman, L. I., Springston, S. R., Daum, P. H., Lee, Y.-N., Nunnermacker, L. J., Senum, G. I., et al. (2008). The Time Evolution of Aerosol Composition Over the Mexico City Plateau. *Atmos. Chem. Phys.* 8:1559–1575, doi:10.5194/acp-8-1559-2008.

Kondo, Y., Miyazaki, Y., Takegawa, N., Miyakawa, T., Weber, R. J., Jimenez, J. L., et al. (2007). Oxygenated and Water-Soluble Organic Aerosols in Tokyo. *J. Geophys. Res.* 112:D01203, doi:10.1029/2006JD007056.

Liu, P. S. K., Deng, R., Smith, K. A., Williams, L. R., Jayne, J. T., Canagaratna, M. R., et al. (2007). Transmission Efficiency of an Aerodynamic Focusing Lens System: Comparison of Model Calculations and Laboratory Measurements for the Aerodyne Aerosol Mass Spectrometer. *Aerosol Sci. Technol.* 41:721–733, doi:10.1080/02786820701422278.

Marcolli, C., Luo, B., and Peter, T. (2004). Mixing of the Organic Aerosol Fractions: Liquids as the Thermodynamically Stable Phases. *J. Phys. Chem. A* 108:2216–2224, doi:10.1021/jp036080l.

Martin, S. T. (2000). Phase Transitions of Aqueous Atmospheric Particles. *Chem. Rev.* 100:3403–3453, doi:10.1021/cr990034t.

Matthew, B. M., Middlebrook, A. M., and Onasch, T. B. (2008). Collection Efficiencies in an Aerodyne Aerosol Mass Spectrometer as a Function of Particle Phase for Laboratory Generated Aerosols. *Aerosol Sci. Technol.* 42:884–898, doi:10.1080/02786820802356797.

Murphy, D. M., Cziczo, D. J., Froyd, K. D., Hudson, P. K., Matthew, B. M., Middlebrook, A. M., et al. (2006). Single-Particle Mass Spectrometry of Tropospheric Aerosol Particles. *J. Geophys. Res.* 111:D23S32, doi:10.1029/2006JD007340.

Nemitz, E., other1, other2, other3, other4, other5, et al. (2011). Aerosol Mass Spectrometer Network Measurements During the EUCAARI/EMEP Intensive Measurement Campaigns. *Atmos. Chem. Phys. Disc.* in prep.

Ng, N. L., Herndon, S. C., Trimborn, A., Canagaratna, M. R., Croteau, P. L., Onasch, T. B., et al. (2011). An Aerosol Chemical Speciation Monitor (ACSM) for Routine Monitoring of the Composition and Mass Concentrations of Ambient Aerosol. *Aerosol Sci. Technol.* 45:780–794, doi:10.1080/02786826.2011.560211.

Park, K., Kittelson, D. B., Zachariah, M. R., and McMurry, P. H. (2004). Measurement of Inherent Material Density of Nanoparticle Agglomerates. *J. Nanoparticle Res.* 6:267–272, doi:10.1023/B:NANO.0000034657.71309.e6.

Perry, R. H., and Green, D. W., eds. (1997). *Perry's Chemical Engineers' Handbook*. McGraw-Hill, New York, NY.

Quinn, P. K., Bates, T. S., Coffman, D., Onasch, T. B., Worsnop, D., Baynard, T., et al. (2006). Impacts of Sources and Aging on Submicrometer Aerosol Properties in the Marine Boundary Layer Across the Gulf of Maine. *J. Geophys. Res.* 111:D23S36, doi:10.1029/2006JD007582.

Rood, M. J., Shaw, M. A., Larson, T. V., and Covert, D. S. (1989). Ubiquitous Nature of Ambient Metastable Aerosol. *Nature* 337:537–539, doi:10.1038/337537a0.

Salcedo, D., Onasch, T. B., Canagaratna, M. R., Dzepina, K., Huffman, J. A., Jayne, J. T., et al. (2007). Technical Note: Use of a Beam Width Probe in an Aerosol Mass Spectrometer to Monitor Particle Collection Efficiency in the Field. *Atmos. Chem. Phys.* 7:549–556, doi:10.5194/acp-7-549-2007.

Salcedo, D., Onasch, T. B., Dzepina, K., Canagaratna, M. R., Zhang, Q., Huffman, J. A., et al. (2006). Characterization of Ambient Aerosols in Mexico City During the MCMA-2003 Campaign with Aerosol Mass Spectrometry: Results from the CENICA Supersite. *Atmos. Chem. Phys.* 6:925–946, doi:10.5194/acp-6-925-2006.

Schwarz, J. P., Gao, R. S., Fahey, D. W., Thomson, D.S., Watts, L. A., Wilson, J. C., et al. (2006). Single-Particle Measurements of Midlatitude Black Carbon and Light-Scattering Aerosols from the Boundary Layer to the Lower Stratosphere. *J. Geophys. Res.* 111:D16207, doi:10.1029/2006JD007076.

Slowik, J. G., Stroud, C., Bottenheim, J. W., Brickell, P. C., Chang, R. Y.-W., Liggio, J., et al. (2010). Characterization of a Large Biogenic Secondary Organic Aerosol Event from Eastern Canadian Forests. *Atmos. Chem. Phys.* 10:2825–2845, doi:10.5194/acp-10-2825-2010.

Takegawa, N., Miyazaki, Y., Kondo, Y., Komazaki, Y., Miyakawa, T., Jimenez, J. L., et al. (2005). Characterization of an Aerodyne Aerosol Mass Spectrometer (AMS): Intercomparison with Other Aerosol Instruments. *Aerosol Sci. Technol.* 39:760–770, doi:10.1080/02786820500243404.

Tang, I. N. (1980). Deliquescence Properties and Particle Size Change of Hygroscopic Aerosols, in *Generation of Aerosols and Facilities for Exposure Experiments*, K. Willeke, ed., Ann Arbor Science Publishers, Ann Arbor, MI, 153–167.

Timonen, H., Aurela, M., Carbone, S., Saarnio, K., Saarikoski, S., Makela, T., et al. (2010). High Time-Resolution Chemical Characterization of the Water Soluble Fraction of Ambient Aerosols with PILS-TOC-IC and AMS. *Atmos. Meas. Tech.* 3:1063–1074, doi:10.5194/amt-3–1063-2010.

Topping, D., Coe, H., McFiggans, G., Burgess, R., Allan, J., Alfarra, M. R., et al. (2004). Aerosol Chemical Characteristics from Sampling Conducted on the Island of Jeju, Korea During ACE Asia. *Atmos. Environ.* 38:2111–2123, doi:10.1016/j.atmosenv.2004.01.022.

Venkatachari, P., Zhou, L., Hopke, P. K., Schwab, J. J., Demerjian, K. L., Weimer, S., et al. (2006). An Intercomparison of Measurement Methods for Carbonaceous Aerosol in Ambient air in New York City. *Aerosol Sci. Technol.* 40:788–795, doi:10.1080/02786820500380289.

Virtanen, A., Joutsensaari, J., Koop, T., Kannosto, J., Yli-Pirila, P., J.Leskinen, et al. (2010). An Amorphous Solid State of Biogenic Secondary Organic Aerosol Particles. *Nature* 467:824–827, doi:10.1038/nature09455.

Warneke, C., Bahreini, R., Brioude, J., Brock, C. A., de Gouw, J. A., Fahey, D. W., et al. (2009). Biomass Burning in Siberia and Kazakhstan as an Important Source for Haze Over the Alaskan Arctic in April 2008. *Geophys. Res. Lett.* 36:L02813, doi:10.1029/2008GL036194.

Weber, R. J., Orsini, D., Daun, Y., Lee, Y.-N., Klotz, P. J., and Brechtel, F. (2001). A Particle-into-Liquid Collector for Rapid Measurement of Aerosol Bulk Chemical Composition. *Aerosol Sci. Technol.* 35:718–725, doi:10.1080/02786820152546761.

Weimer, S., Drewnick, F., Hogrefe, O., Schwab, J. J., Rhoads, K., Orsini, D., et al. (2006). Size-Selective Nonrefractory Ambient Aerosol Measurements During the Particulate Matter Technology Assessment and Characterization Study - New York 2004 Winter Intensive in New York City. *J. Geophys. Res.* 111:D18305, doi:10.1029/2006JD007215.

Wexler, A. S., and Clegg, S. L. (2002). Atmospheric Aerosol Models for Systems Including the Ions H+, NH4+, Na+, SO42-, NO3-, Cl-, Br-, and H2O. *J. Geophys. Res.* 107:4207, doi:10.1029/2001JD000451.

Zelenyuk, A., Imre, D., and Cuadra-Rodriguez, L. A. (2006). Evaporation of Water from Particles in the Aerodynamic Lens Inlet: An Experimental Study. *Anal. Chem.* 78:6942–6947, doi:10.1021/ac061184o.

Zelenyuk, A., Imre, D., Han, J. H., and Oatis, S. (2008). Simultaneous Measurements of Individual Ambient Particle Size, Composition, Effective Density, and Hygroscopicity. *Anal. Chem.* 80:1401–1407, doi:10.1021/ac701723v.

Zhang, Q., Jimenez, J. L., Canagaratna, M. R., Allan, J. D., Coe, H., Ulbrich, I., et al. (2007a). Ubiquity and Dominance of Oxygenated Species in Organic Aerosols in Anthropogenically-Influenced Northern Hemisphere Midlatitudes. *Geophys. Res. Lett.* 34:L13801, doi:10.1029/2007GL029979.

Zhang, Q., Jimenez, J. L., Worsnop, D. R., and Canagaratna, M. (2007b). A Case Study of Urban Particle Acidity and Its Ifluence on Secondary Organic Aerosol. *Environ. Sci. Technol.* 41:3213–3219, doi:10.1021/es061812j.

Zhang, X., Smith, K. A., Worsnop, D. R., Jimenez, J. L., Jayne, J. T., Kolb, C. E., et al. (2004). Characterization of Particle Beam Collimation: Part II Integrated Aerodynamic Lens-Nozzle System. *Aerosol Sci. Technol.* 38:619–638, doi:10.1080/02786820490479833.

Supplemental Information for "Evaluation of Composition-Dependent Collection Efficiencies for the Aerodyne Aerosol Mass Spectrometer using Field Data"
by Ann M. Middlebrook, Roya Bahreini, Jose L. Jimenez, and Manjula R. Canagaratna

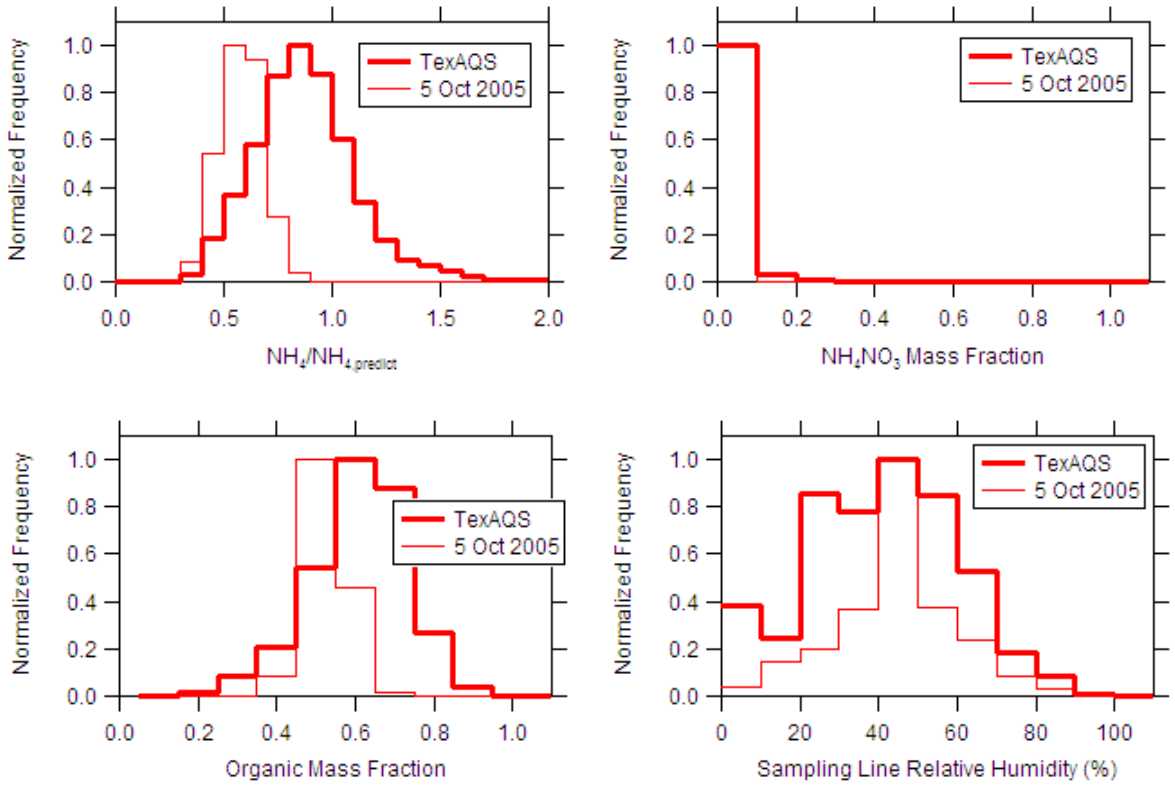

FIG S1. Chemical characterization of the measured aerosol mass during the TexAQS-II study depicted in the ratio of measured to predicted ammonium (top left panel), the ammonium nitrate mass fraction (top right panel), the organic mass fraction (bottom left panel), and the sampling line relative humidity (bottom right panel).The flight on 5 Oct 2005 is also depicted since it was a flight with higher than average acidity and is discussed more fully in the text.

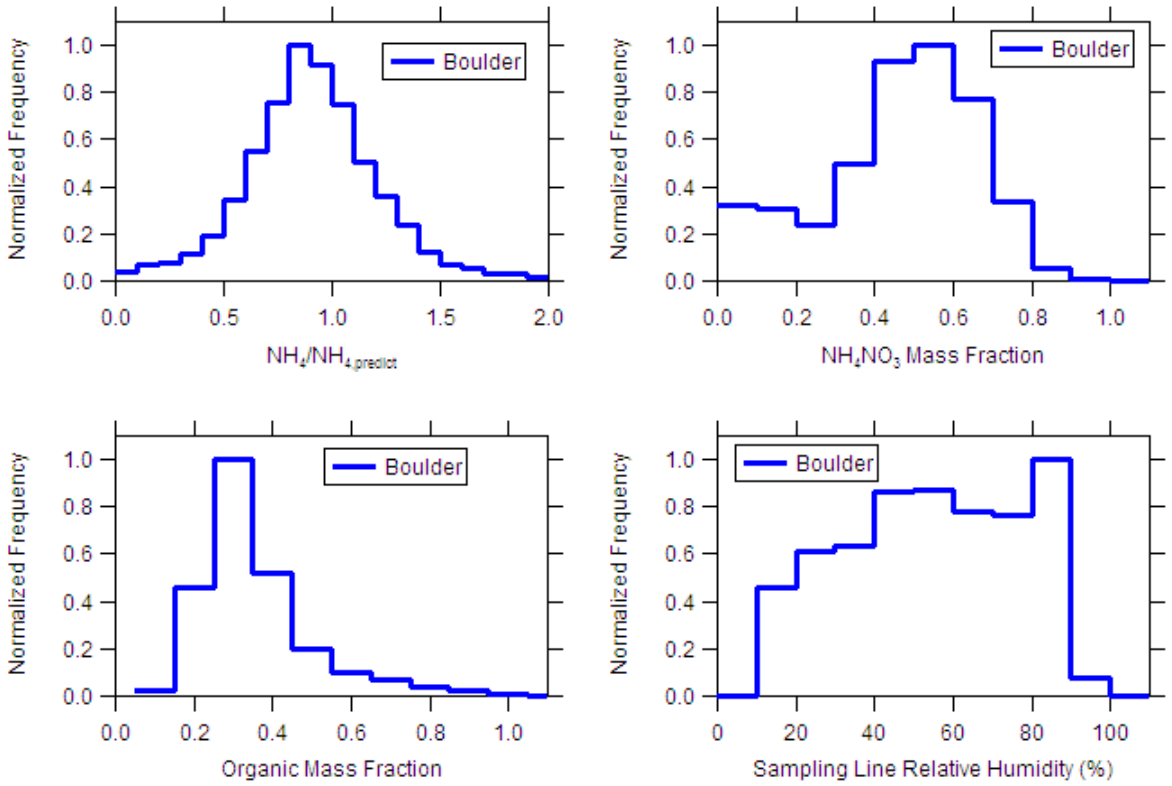

FIG S2. Chemical characterization of the measured aerosol mass during the Boulder winter study depicted in the ratio of measured to predicted ammonium (top left panel), the ammonium nitrate mass fraction (top right panel), the organic mass fraction (bottom left panel), and the sampling line relative humidity (bottom right panel).

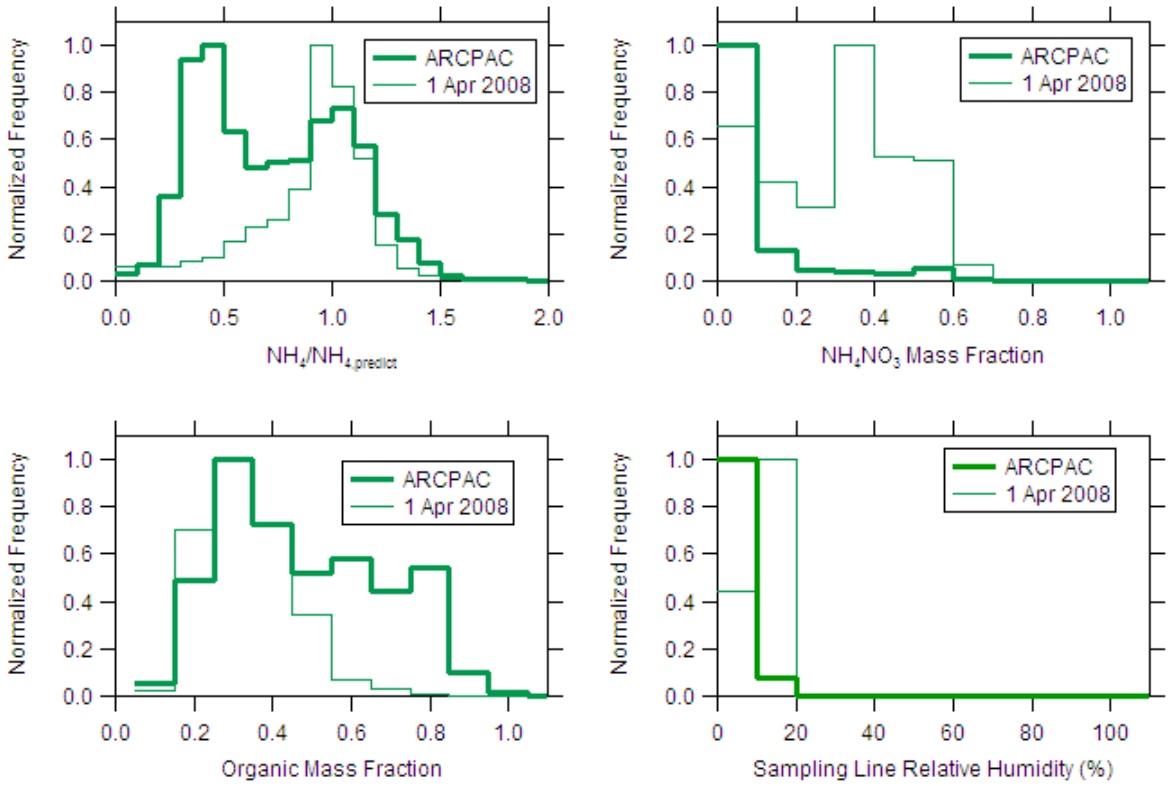

FIG S3. Chemical characterization of the measured aerosol mass during the ARCPAC study depicted in the ratio of measured to predicted ammonium (top left panel), the ammonium nitrate mass fraction (top right panel), the organic mass fraction (bottom left panel), and the sampling line relative humidity (bottom right panel). The flight on 1 Apr 2008 is also depicted since it was a flight over Colorado with higher than average nitrate content and is discussed more fully in the text.

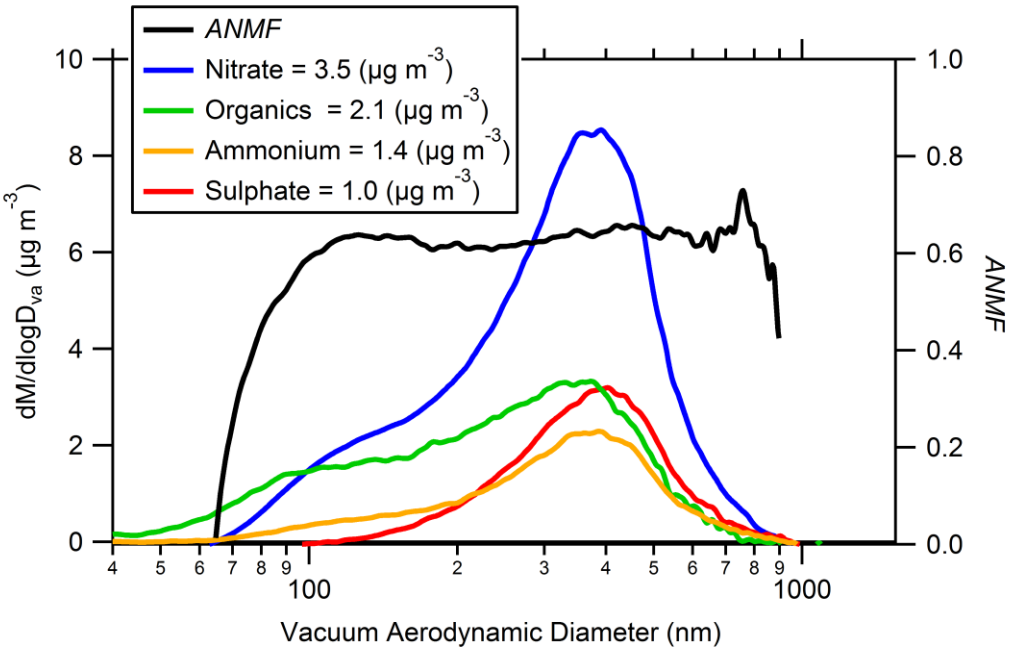

FIG S4. Average mass concentrations as a function of vacuum aerodynamic diameter (d_{va}) for various species measured with the AMS in Boulder, CO from 26 Jan 2005 to 9 Feb 2005. These concentrations were calculated using *CE* = 0.5 for all species. The ammonium nitrate mass fraction for the average distribution is approximately 0.65 over the size range containing most of the aerosol mass.

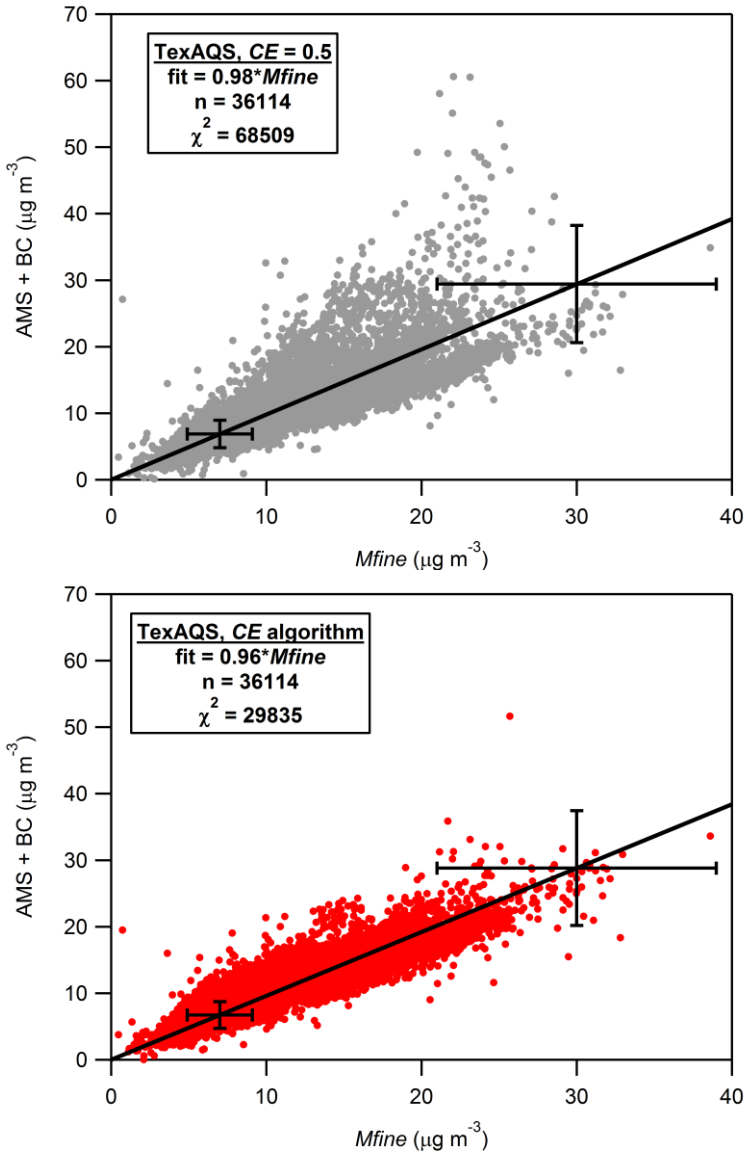

Fig. S5. Mass from the AMS plus black carbon (BC) versus the fine particulate mass (*Mfine*) from the TexAQS field study. The default *CE* is used to calculate the AMS mass in the top panel and the *CE* algorithm described in this manuscript was used in the bottom panel. The linear fit is an orthogonal distance regression with an intercept of 0. The difference in slopes between the two is not significant. The decrease in χ^2 indicates that the data obtained using the *CE* algorithm is better represented by a linear relationship to *Mfine* than the data obtained using the default *CE*.

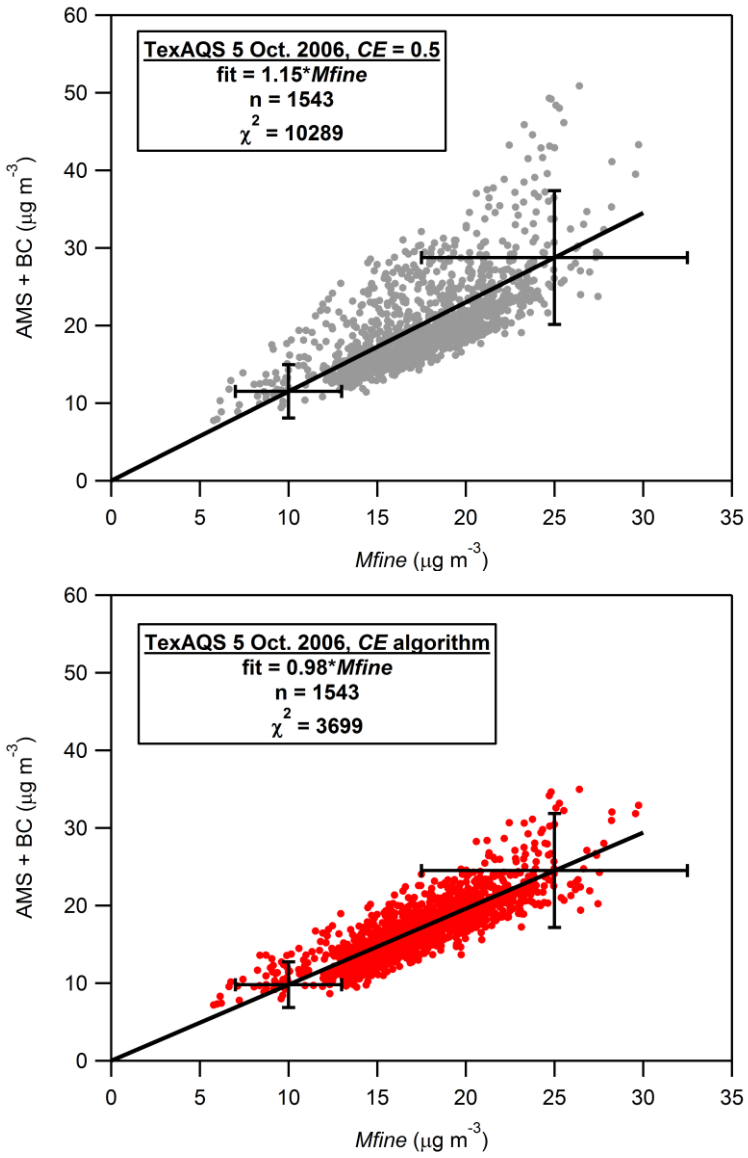

Fig. S6. Mass from the AMS plus black carbon (BC) versus the fine particulate mass (*Mfine*) from 5 Oct. 2006 during the TexAQS field study. The default *CE* is used to calculate the AMS mass in the top panel and the *CE* algorithm described in this manuscript was used in the bottom panel. The linear fit is an orthogonal distance regression with an intercept of 0. The slope from the fit for the data using the *CE* algorithm is closer to one than the slope from the fit for the data using the default *CE*. The decrease in χ^2 indicates that the data obtained using the *CE* algorithm is better represented by a linear relationship to *Mfine* than the data obtained using the default *CE*.

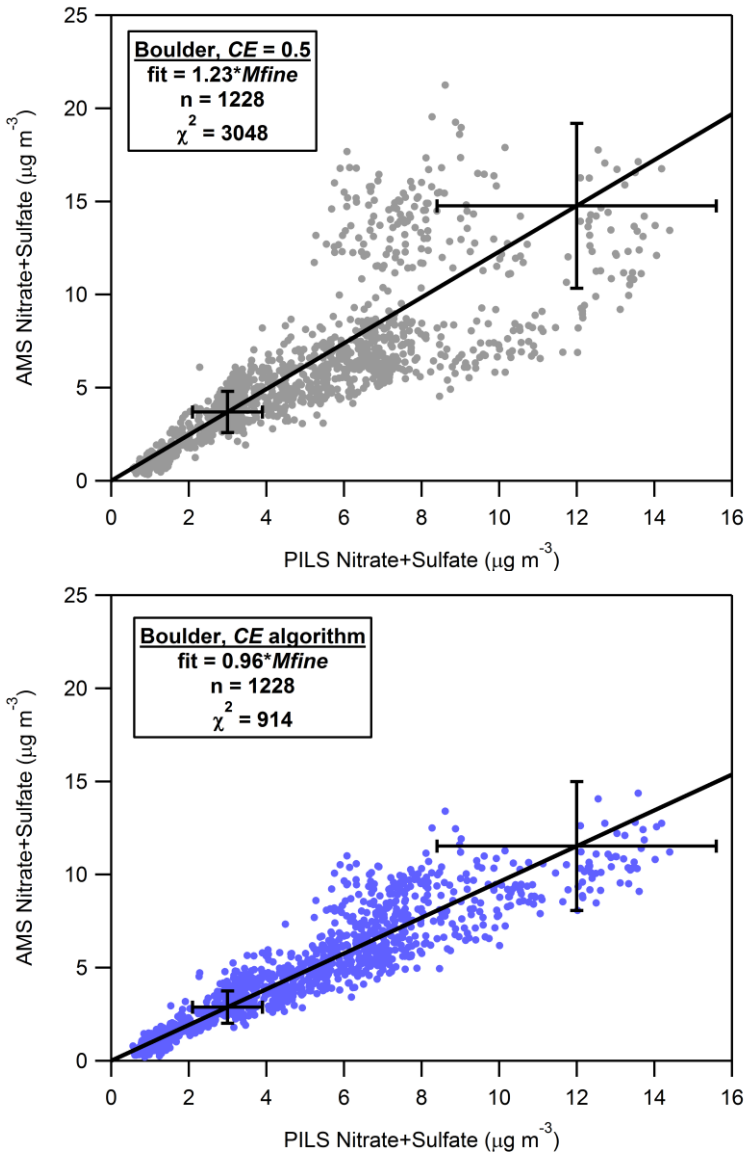

Fig. S7. Nitrate plus sulfate mass from the AMS versus nitrate plus sulfate mass from the PILS instrument during the field study in Boulder, CO. The default *CE* is used to calculate the AMS mass in the top panel and the *CE* algorithm described in this manuscript was used in the bottom panel. The linear fit is an orthogonal distance regression with an intercept of 0. The slope from the fit for the data using the *CE* algorithm is closer to one than the slope from the fit for the data using the default *CE*. The decrease in χ^2 indicates that the data obtained using the *CE* algorithm is better represented by a linear relationship to *Mfine* than the data obtained using the default *CE*.

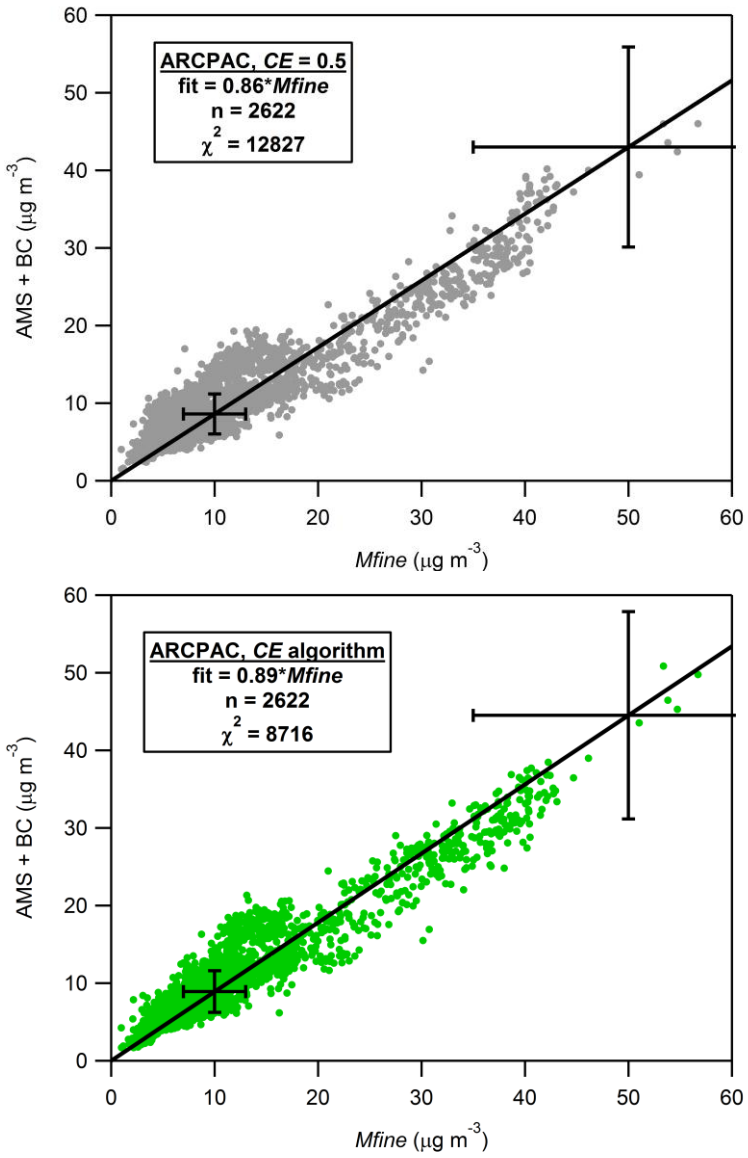

Fig. S8. Mass from the AMS plus black carbon (BC) versus the fine particulate mass (*Mfine*) from the ARCPAC study. The default *CE* is used to calculate the AMS mass in the top panel and the *CE* algorithm described in this manuscript was used in the bottom panel. The linear fit is an orthogonal distance regression with an intercept of 0. The slope from the fit for the data using the *CE* algorithm is closer to one than the slope from the fit for the data using the default *CE*. The decrease in χ^2 indicates that the data obtained using the *CE* algorithm is better represented by a linear relationship to *Mfine* than the data obtained using the default *CE*.

IGOR Procedure File (ipf) for determining the composition- (phase-) dependent *CE* using Equations 3-7.

```
Function CalcCE_fPhase(NH4_DL,CE_lowNH4)
    Variable NH4_DL,CE_lowNH4
    //  NH4_DL = ammonium detection limit
    //  CE_lowNH4 = CE for points where ammonium is below its detection limit

    //  Prior to running this procedure, all species must be calculated using CE=1.
    //  The sampling line relative humidity (if measured) should be named "RH_SL"

    wave SO4, NH4, NO3, Chl, org, RH_SL

    //    Create waves of each species to smooth for the calculations.
    duplicate/o SO4 SO4_CE1
    duplicate/o NH4 NH4_CE1
    duplicate/o NO3 NO3_CE1
    duplicate/o Chl Chl_CE1
    duplicate/o org org_CE1

    Smooth 1, SO4_CE1,NH4_CE1,NO3_CE1,Chl_CE1, org_CE1

    Variable i
    Duplicate/o SO4 PredNH4_CE1, NH4_MeasToPredict, ANMF
    Duplicate/o SO4 CE_dry,CE_fPhase
    CE_dry=nan
    CE_fPhase=nan

    //    Equation 3
    PredNH4_CE1=18*(SO4_CE1/96*2+NO3_CE1/62+Chl_CE1/35.45)
    NH4_MeasToPredict=NH4_CE1/PredNH4_CE1

    //    Equation 5
    ANMF=(80/62)*NO3_CE1/(NO3_CE1+SO4_CE1+NH4_CE1+Org_CE1+Chl_CE1)

    //    Calculate the dry collection efficiency, CE_dry
```

```
For (i=0;i<(numpnts(SO4_CE1)+1);i+=1)
    //  Nan negative NH4_MeasToPredict points
    If (NH4_MeasToPredict[i]<0)
        NH4_MeasToPredict[i]=nan
    EndIf

    //  Nan ANMF points if negative or more than 1
    If (ANMF[i]<0)
        ANMF[i]=nan
    ElseIf (ANMF[i]>1)
        ANMF[i]=nan
    EndIf

    If (PredNH4_CE1[i]<NH4_DL)
        //  In general, do not calculate CE for these points.
        CE_dry[i]=nan
        //  In the CE paper, applied CE for low ammonium mass
        //  CE_dry[i]=CE_lowNH4
    ElseIf (NH4_MeasToPredict[i]>=0.75)
        //  Apply Equation 4
        CE_dry[i]= 0.0833+0.9167*ANMF[i]
    ElseIf (NH4_MeasToPredict[i]<0.75)
        //  Apply Equation 6
        CE_dry[i]= 1-0.73*NH4_MeasToPredict[i]
    EndIf
EndFor

//  Make CE_dry between 0.45 and 1
CE_dry=min(1,(max(0.45,CE_dry)))

If (WaveExists(RH_SL)==1)
    //  Apply Equation 7
    CE_fPhase=(5*CE_dry-4)+(1-CE_dry)/20*RH_SL
    For (i=0;i<numpnts(CE_fPhase)+1;i+=1)
        If (RH_SL[i]<80 || numtype(RH_SL[i])==2 )
            CE_fPhase[i]=CE_dry[i]
```

```
            EndIf
        EndFor
    Else
        CE_fPhase=CE_dry
    EndIf

    KillWaves SO4_CE1,NH4_CE1,NO3_CE1,Chl_CE1, org_CE1, PredNH4_CE1
End Function
```